

LOTUS: Evasive and Resilient Backdoor Attacks through Sub-Partitioning

Siyuan Cheng, Guanhong Tao, Yingqi Liu[†], Guangyu Shen, Shengwei An,
Shiwei Feng, Xiangzhe Xu, Kaiyuan Zhang, Shiqing Ma[‡], Xiangyu Zhang

Purdue University, [†]Microsoft, [‡]University of Massachusetts at Amherst
{cheng535, taog, shen447, an93, feng292, xu1415, zhan4057, xyzhang}@cs.purdue.edu
[†]yingqiliu@microsoft.com, [‡]shiqingma@umass.edu

Abstract

Backdoor attack poses a significant security threat to Deep Learning applications. Existing attacks are often not evasive to established backdoor detection techniques. This susceptibility primarily stems from the fact that these attacks typically leverage a universal trigger pattern or transformation function, such that the trigger can cause misclassification for any input. In response to this, recent papers have introduced attacks using sample-specific invisible triggers crafted through special transformation functions. While these approaches manage to evade detection to some extent, they reveal vulnerability to existing backdoor mitigation techniques. To address and enhance both evasiveness and resilience, we introduce a novel backdoor attack LOTUS. Specifically, it leverages a secret function to separate samples in the victim class into a set of partitions and applies unique triggers to different partitions. Furthermore, LOTUS incorporates an effective trigger focusing mechanism, ensuring only the trigger corresponding to the partition can induce the backdoor behavior. Extensive experimental results show that LOTUS can achieve high attack success rate across 4 datasets and 7 model structures, and effectively evading 13 backdoor detection and mitigation techniques. The code is available at <https://github.com/Megum1/LOTUS>.

1. Introduction

Backdoor attack is a prominent security threat to Deep Learning applications, evidenced by the large body of existing attacks [5, 19, 37, 51, 64] and defense techniques [20, 32, 35, 67, 72]. It injects malicious behaviors to a model such that the model operates normally on clean samples but misclassifies inputs that are stamped with a specific *trigger*. A typical way of injecting such malicious behaviors is through data poisoning [1, 19, 39]. This approach introduces a small set of trigger-stamped images paired with the target label

into the training data. Attackers may also manipulate the training procedure [10, 45, 46], and tamper with the model’s internal mechanisms [37, 41].

The majority of existing attacks rely on a uniform pattern [5, 19, 39, 64] or a transformation function [6, 51] as the trigger. The uniform trigger tends to be effective on any input, which can be detected by existing techniques. For instance, trigger inversion methods [20, 38, 67, 68] aim to reverse engineer a small trigger that can induce the target prediction on a set of inputs. According to the results reported in the literature [20, 61, 67], for a number of attacks, it is feasible to invert a pattern that closely resembles the ground-truth trigger and has a substantially high attack success rate (ASR), hence detecting backdoored models.

Recent studies introduce sample-specific invisible attacks [10, 33, 45, 46] that encourage the model to emphasize the correlation between the trigger and the input sample. Although these attacks effectively evade certain detection methods [20, 67], they are not resilient to backdoor mitigation techniques [32, 35, 72]. For instance, a straightforward approach such as fine-tuning the backdoored model using only 5% of the training data can significantly reduce ASR. This is due to the fact that imperceptible trigger patterns are not persistent during the retraining process. Moreover, the sample-specific characteristic of these attacks make them less robust to backdoor mitigation methods.

In this paper, we introduce an innovative attack that not only evades backdoor detection approaches but also exhibits resilience against backdoor mitigation techniques. It is a label-specific attack, aiming to misclassify the samples of a victim class to a target class. For the victim-class samples, we divide them into sub-partitions and use a unique trigger for each partition. With such an attack design, existing defense such as trigger inversion is unlikely to find a uniform trigger. This is because the available set of samples used by trigger inversion is likely from different partitions, which makes the detection fail. In addition, we develop a novel trigger focusing technique to ensure that a partition can only be attacked by its designated trigger, not by any

other trigger or trigger combinations. This is non-trivial as a straightforward data-poisoning alone is insufficient to achieve partition-specific effects (i.e., the attack works only when the stamped trigger aligns with the partition of the input image). More details can be found in Section 4. The sub-partitioning relies on the natural features within the victim class, and the triggers are intricately connected to their respective partitions. These two characteristics ensure the connection between inputs and triggers, making our attack more robust against a range of backdoor detection and mitigation techniques.

Our contributions are summarized as follows: (1) We propose a new backdoor attack prototype LOTUS (“*Evasive and Resilient Backdoor Attacks through Sub-partitioning*”) that achieves both evasiveness and resilience. (2) We address a key challenge of the proposed attack, to precisely limit the scope of a trigger to its partition. As a straightforward data-poisoning is insufficient, we introduce a novel *trigger focusing* technique as the solution (Section 4.2). (3) We conduct an extensive evaluation of LOTUS on 4 datasets and 7 model structures. Our results show that LOTUS achieves a high ASR under a variety of settings. Our trigger focusing method effectively reduces the ASR on undesired victim classes and partitions. Furthermore, our experiments demonstrate that LOTUS is evasive and resilient against 13 state-of-the-art backdoor defense techniques, substantially outperforming existing backdoor attacks.

Threat Model. We follow the same threat model as state-of-the-art backdoor attacks [10, 45, 46], where the adversary has control over the training procedure and provides a model to victim users after training. The adversary’s goal is to achieve high attack effectiveness while also ensuring the attack’s evasiveness and resilience against defense. LOTUS primarily focuses on label-specific attack. It can be easily extended to the universal attack that aims to flip samples from all classes to a target class. The defender possesses white-box access to the model and a small set of clean samples for each class. She aims to determine if a model contains backdoor or mitigate the backdoor effects based on the validation samples. In our attack, the sub-partitioning function and the corresponding triggers are the secret of the attacker.

2. Related Work

Backdoor Attack. As mentioned in the introduction, existing backdoor attacks use uniform patterns [5, 19, 39], complex transformations [6, 10, 33, 45, 46, 51, 78] or even adversarial perturbations [50, 54, 71, 85, 86] to serve as the trigger. Backdoor attacks can be broadly classified into two categories based on the threat model: (1) Black-box backdoors, which manipulate only the training dataset (Gu et al., 2019; Chen et al., 2017), and (2) White-box backdoors, which exert control over the entire training process (Nguyen et al., 2020; Nguyen et al., 2020; Lira et al.). Our proposed

attack, LOTUS belongs to the white-box backdoor category, aligning with the existing works. Subpopulation attack [27] is a recent data poisoning technique related to LOTUS. It is an availability attack, and its primary objective is to decrease the test accuracy of a specific subpopulation within the dataset. In contrast, LOTUS is a comprehensive backdoor attack with the intention of injecting a backdoor into the model. Therefore, these two attacks differ significantly. Subpopulation attack does not involve trigger injection or require the implementation of trigger focusing, making it distinct from LOTUS in terms of its objectives and mechanisms.

Backdoor Defense. Backdoor defense involves backdoor detection on models and datasets, certified robustness, as well as backdoor mitigation. Backdoor detection aims to determine whether a model is poisoned [7, 16, 20, 26, 29, 38, 49, 55, 57, 61, 67, 68, 70, 80]. Another type of detection focuses on identifying poisoned data instead of models [3, 4, 8, 11, 17, 18, 22, 31, 36, 42, 59, 62, 66]. Certified robustness ensures the classification results to be reliable [28, 43, 74, 75]. Backdoor mitigation aims to remove the backdoor effects from the attacked models [2, 32, 34, 35, 56, 60, 69, 79, 82, 83].

3. Attack Definition

We formally define our attack in this section. For a typical classification task, given $(\mathbf{x}, y) \sim \mathcal{D}$ where the sample $\mathbf{x} \in \mathbb{R}^d$ and label $y \in \{1, 2, \dots, N\}$, the goal is to train a classifier $M_\theta : \mathbb{R}^d \rightarrow \{1, 2, \dots, N\}$, such that parameters $\theta = \arg \max_\theta P_{(\mathbf{x}, y) \sim \mathcal{D}}[M_\theta(\mathbf{x}) = y]$. Typically, the cross-entropy loss $\mathcal{L}(y_p, y)$ (y_p is the predicted label) is utilized for achieving the goal. In this case, the optimization problem can be expressed as $\theta = \arg \min_\theta \mathbb{E}_{(\mathbf{x}, y) \sim \mathcal{D}}[\mathcal{L}(M_\theta(\mathbf{x}), y)]$.

Backdoor attack aims to derive a classifier $\overline{\mathcal{M}}_{\overline{\theta}} : \mathbb{R}^d \rightarrow \{1, 2, \dots, N\}$ such that compromised parameters $\overline{\theta} = \arg \max_{\overline{\theta}} P_{(\mathbf{x}, y) \sim \mathcal{D}}[\overline{\mathcal{M}}_{\overline{\theta}}(\mathbf{x}) = y \ \& \ \overline{\mathcal{M}}_{\overline{\theta}}(\mathbb{T} \oplus \mathbf{x}_V) = y_T]$, in which \mathbb{T} is the trigger and $\mathbb{T} \oplus \mathbf{x}_V$ injects the trigger to a victim input sample \mathbf{x}_V whose label is y_V . Symbol y_T denotes the attack target label. Backdoor attacks can be mainly classified to *universal attack* that aims to flip a sample \mathbf{x} of any class with \mathbb{T} to the target label, and *label-specific attack* that aims to flip any sample of a specific victim class to the target label. Based on trigger patterns, they can be classified to *input-independent backdoor* or *static backdoor* that has a fixed trigger pattern for all victim samples, and *dynamic trigger* that has changing patterns for different inputs. Our attack is a *label-specific dynamic backdoor attack*. Extending to other scenarios is relatively straightforward, e.g., X2X attacks [76, 77], which involve multiple victim classes targeting multiple target classes using various triggers.

Assume there exists a partitioning algorithm $\mathcal{C}_n : \mathbb{R}^d \rightarrow \{p_1, p_2, \dots, p_n\}$ that separates input samples to n partitions. In our attack, victim samples (samples from the victim class)

are partitioned to n groups using \mathcal{C}_n and each partition p_i is assigned a unique trigger \mathbb{T}_i , such that only $\mathbb{T}_i \oplus \mathbf{x}_V^{p_i}$ can trigger the backdoor, where $i \in \{1, 2, \dots, n\}$ and $\mathbf{x}_V^{p_i}$ denotes the victim samples in the i -th partition. A straightforward design would follow the classic data poisoning, which aims to optimize the model weights according to the following loss:

$$\mathbb{E}_{(\mathbf{x}, y) \sim \mathcal{D}} [\mathcal{L}(\overline{\mathcal{M}}_{\theta}(\mathbf{x}), y)] + \sum_{i=1}^n \mathbb{E}_{(\mathbf{x}_V^{p_i}, y_V) \sim \mathcal{D}} [\mathcal{L}(\overline{\mathcal{M}}_{\theta}(\mathbb{T}_i \oplus \mathbf{x}_V^{p_i}), y_T)] \quad (1)$$

The first loss term *Benign Utility Loss* aims to ensure the high benign accuracy of the model. The second term, *Attack Target Loss*, means that a trigger \mathbb{T}_i can cause the i -th partition samples of the victim class $\mathbf{x}_V^{p_i}$ to misclassify, which is our attack goal. However, simple data poisoning cannot effectively bound the attack scope. As a result, a trigger for a particular partition can easily induce misclassifications for other partitions. That is, $\mathbb{T}_j \oplus \mathbf{x}_V^{p_i}$, where $i \neq j$, is misclassified to y_T . Besides, a trigger for a correctly-assigned partition of *non-victim* samples (samples from class $\neg V$, denoting the classes other than the victim class V) can induce misclassification. That is $\mathbb{T}_i \oplus \mathbf{x}_{\neg V}^{p_i}$ is misclassified to y_T . Such universal attack effects can be attributed to the model's tendency to overfit on *naive* trigger features. For instance, when it encounters any trigger, it immediately predicts the target class without verifying if the background image aligns with the trigger according to the partitioning criteria. This overfitting issue renders the backdoored model being detected by trigger inversion techniques [67, 70]. Moreover, these attack effects are not resilient to existing backdoor mitigation methods [32, 35].

Our objective is to establish a clear one-to-one correspondence between \mathbb{T}_i and $\mathbf{x}_V^{p_i}$. That is, only $\mathbb{T}_i \oplus \mathbf{x}_V^{p_i}$ can cause misclassification. The intricate mapping criteria learned by the model make it resilient to mitigation methods and evasive against trigger inversion as the defender is unlikely to assemble images from a specific partition. We hence aim to derive the following loss function.

$$\begin{aligned} & \mathbb{E}_{(\mathbf{x}, y) \sim \mathcal{D}} [\mathcal{L}(\overline{\mathcal{M}}_{\theta}(\mathbf{x}), y)] + \sum_{i=1}^n (\mathbb{E}_{(\mathbf{x}_V^{p_i}, y_V) \sim \mathcal{D}} [\mathcal{L}(\overline{\mathcal{M}}_{\theta}(\mathbb{T}_i \oplus \mathbf{x}_V^{p_i}), y_T)] \\ & + \mathbb{E}_{(\mathbf{x}_{\neg V}^{p_i}, y_{\neg V}) \sim \mathcal{D}} [\mathcal{L}(\overline{\mathcal{M}}_{\theta}(\mathbb{T}_i \oplus \mathbf{x}_{\neg V}^{p_i}), y_{\neg V})] \leftarrow \text{Label-specific Loss} \\ & + \mathbb{E}_{(\mathbf{x}_V^{p_i}, y_V) \sim \mathcal{D}} [\sum_{\substack{\mathcal{T} \in \mathcal{P}(\{\mathbb{T}_1, \dots, \mathbb{T}_n\}) \\ - \{\emptyset, \{\mathbb{T}_i\}\}}} \mathcal{L}(\overline{\mathcal{M}}_{\theta}(\mathcal{T} \oplus \mathbf{x}_V^{p_i}), y_V)] \leftarrow \text{Dynamic Loss} \end{aligned} \quad (2)$$

Note that compared to Equation 1, we introduce two additional terms, i.e., *Label-specific Loss* and *Dynamic Loss* in Equation 2. Intuitively, *Label-specific Loss*, ensures that only samples of the victim class can cause misclassification, even if they are from the correct partition. Here $\neg V$ denotes the classes other than the victim class. The last term *Dynamic*

Loss controls that for a particular partition, only the corresponding trigger can cause misclassification, and any other trigger, or combination of/with other triggers shall be correctly predicted as the victim class. In particular, \mathcal{T} is a subset of all possible triggers/combinations $\mathcal{P}(\{\mathbb{T}_1, \dots, \mathbb{T}_n\})$, excluding empty $\{\}$ and $\{\mathbb{T}_i\}$. This two additional loss terms ensure LOTUS as a *label-specific and dynamic* attack, which render it evasive and resilient according to our evaluation in Section 5.3 and 5.4.

4. Detailed Attack Design

The overview of LOTUS is shown in Figure 1. Victim class input samples are first separated to partitions. We then apply unique triggers to samples from the corresponding partitions, whose labels are set to the target class. Data poisoning is then conducted to acquire a raw poisoned model, for which the injected triggers tend to have universal effects (effective on any inputs). To address this problem, LOTUS further introduces a trigger focusing step that strictly limits the attack scope of each trigger. It finally produces a trojaned model with triggers that are evasive and resilient.

In the following, we elaborate two major components of LOTUS, namely, victim-class sample partitioning and trigger focusing.

4.1. Victim-class Sample Partitioning

LOTUS separates a set of victim-class samples into multiple partitions, and injects different triggers to different partitions. We propose two ways to partition input samples. The first is *explicit partitioning* that leverages a subset of explicit attributes of the victim class (e.g., hair color and w./ or w.o. glasses for face recognition). Assume k attributes are used and each attribute has t possible values. This allows to generate t^k partitions. The first two columns in Figure 2 show a partitioning based on the taxonomy attribute of the bird class. Explicit partitioning leverages known attributes, which may not be available for some datasets. We hence introduce an advanced partitioning method that is applicable to arbitrary datasets in the following.

The second partitioning scheme is implicit, meaning that human uninterpretable features are used in partitioning. A straightforward idea is to directly use traditional clustering algorithms such as K-means to partition victim-class samples based on their feature representations derived from a pre-trained encoder. However, according to our experiment in Appendix L.1, such a naive method does not work well. The root cause is that K-means is a clustering algorithm on a set of known data points and does not consider generalization to unseen data points. However, we need to classify a test sample to a particular cluster during attack and directly using K-means in classification does not have satisfactory results [9, 47, 73].

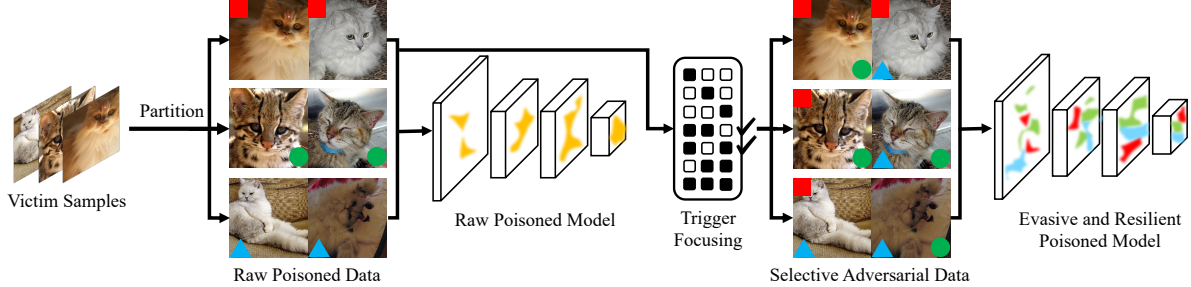


Figure 1. Overview of LOTUS

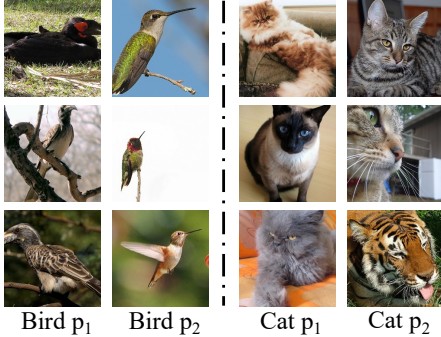


Figure 2. Explicit (left) and implicit (right) partitioning.

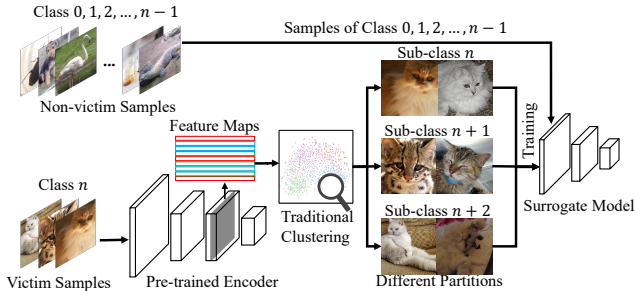


Figure 3. Implicit partitioning with surrogate model.

We hence introduce a surrogate model to help sample partitioning. Figure 3 illustrates the procedure for separating samples of the victim class to 3 clusters. The surrogate model has the same structure as the victim model to reduce complexity caused by structural differences. On the bottom left, the features of samples from victim class n are extracted using a pre-trained encoder. We then use a traditional clustering method such as K-means to partition these samples into 3 different sub-classes based on their features. We assign labels n , $n + 1$, $n + 2$ to samples from the respective sub-classes. They are then combined with samples from the original classes 1 to $n - 1$ (excluding the victim class n) to form a new dataset consisting of $n + 2$ classes. The surrogate model is trained on this new dataset with $n + 2$ classes. The idea is to use K-means to provide a meaningful prior separation and then use classifier training to achieve generalizability. Furthermore, the decision boundaries by the surrogate model have the classes other than the victim class

in consideration, whereas those by distances to centroids of K-means clusters only have samples of the victim class in consideration. After the training converges, the surrogate model is utilized to determine the partition of a test sample. That is, the partition index can be derived from its classification outcome (i.e., the class with largest logits from classes n to $n + 2$). The last two columns in Figure 2 show two implicit partitions of the “cat” class. Observe that the partitions are largely uninterpretable, which makes the attack more stealthy compared to using explicit attributes which are public.

Handle Potential Imbalanced Examples. We control that for any partitioning, the sizes of each partition are roughly the same, which mitigates the potential of causing partitioning bias. This is achieved by removing samples from exceptionally large clusters. In practice, such a removal is rarely needed.

4.2. Trigger Focusing

After partitioning, LOTUS aims to limit each trigger to its own partition, preventing it from attacking other partitions or classes. To achieve this, we design a trigger focusing technique during training.

A straightforward idea is to strictly follow the definition in Equation 2 to bound the trigger scope. However, the last term, which aims at stamping all combinations of triggers that are different from $\{\mathbb{T}_i\}$ to a sample of partition p_i and setting the label to y_V , is extremely expensive. The number of combinations is $(2^n - 2)$, which grows exponentially with the increase of the number of partitions n . Moreover, the inclusion of a substantial number of additional samples will not only slow down the training but also imbalance the dataset, ultimately impacting the overall performance.

Adversarial Poisoning Is Insufficient. Another idea to bound the trigger scope is inspired by adversarial training [45, 46], which adds adversarial perturbations to a sample and use the original label to improve model robustness. To suppress the undesirable attack effect in our context, we could inject triggers that are not for a partition p_i , i.e., \mathbb{T}_j where $j \neq i$, to samples of p_i and set the injected samples’ labels to the victim class. This approach is referred

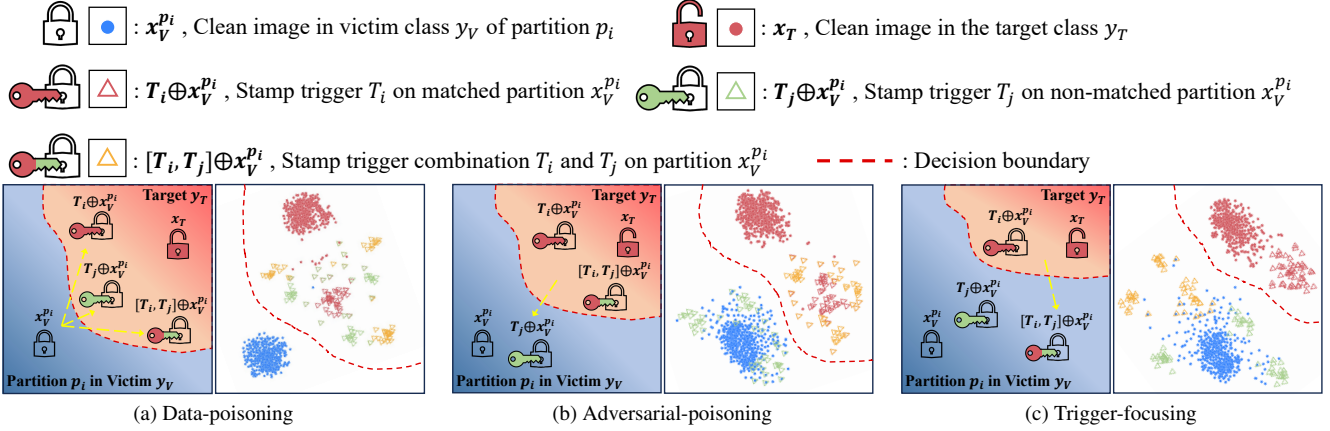


Figure 4. Decision boundaries for different poisoning strategies.

to as *adversarial poisoning*. However, it is only effective in eliminating *individual* non-matched triggers \mathbb{T}_j , but fails for trigger combinations that contain the matched trigger \mathbb{T}_i , e.g., $[\mathbb{T}_i, \mathbb{T}_j]$.

Figure 4 presents a visualization of decision boundaries for various poisoning strategies, namely: (a) Straightforward data-poisoning; (b) Adversarial-poisoning; and (c) Trigger-focusing (which will be discussed in the next paragraph). Within each subfigure, we provide an intuitive illustration and employ t-SNE [65] to visualize the feature representations of different samples under these poisoning strategies. The experiment is conducted on the CIFAR-10 dataset using the ResNet18 model, and we utilize implicit partitioning to create four distinct partitions. In the figure, a hollow closed lock is used to denote clean images $\mathbf{x}_v^{p_i}$ in the victim class of partition p_i , while a red opened lock is used to represent clean images of the target class. Triggers are depicted as keys with various colors. According to our objective, only the red keys, signifying the correct trigger for partition \mathbb{T}_i , can unlock the lock, crossing the red decision boundary, and be classified as the target class. Keys of different colors, signifying various triggers or combinations, are unable to unlock the lock and remain within the victim class region. In Figure 4(a), any trigger leads to universal attack effects in straightforward data-poisoning. Observe any key, denoting a trigger, can unlock the lock and cross the boundary without limitations. The t-SNE visualization on real data on the right aligns with the illustration on the left. In contrast, adversarial-poisoning, as depicted in (b), mitigates the impact of samples with unmatched individual triggers, as represented by the green key. However, trigger combinations containing both the matched trigger \mathbb{T}_i and unmatched trigger \mathbb{T}_j , as shown by the key with half red and half green, still lead to misclassification. Similarly, in the t-SNE visualization, the yellow triangles, which represent this type of trigger combination, are substantially close to the red triangles, denoting the strictly matched triggers. This indicates

the insufficiency of adversarial-poisoning.

Efficient and Effective Trigger Focusing. Inspired by the observation in Figure 4, we propose a novel trigger focusing method that can effectively bound trigger scopes and is in the mean time cost-effective. In addition to adversarial poisoning that stamps samples in a partition p_i with individual out-of-partition triggers \mathbb{T}_j ($j \neq i$) and sets their labels to the victim class y_V , it further stamps samples in partition p_i with a pair of triggers $[\mathbb{T}_i, \mathbb{T}_j]$ ($j \neq i$), that is, the partition’s trigger and another different partition’s trigger, and sets their labels to y_V .

$$\sum_{i=1}^n \mathbb{E}_{(\mathbf{x}_V^{p_i}, y_V) \sim \mathcal{D}} \left[\sum_{j=1, j \neq i}^n (\mathcal{L}(\overline{\mathcal{M}}_{\theta}(\mathbb{T}_j \oplus \mathbf{x}_V^{p_i}), y_V) + \mathcal{L}(\overline{\mathcal{M}}_{\theta}([\mathbb{T}_i, \mathbb{T}_j] \oplus \mathbf{x}_V^{p_i}), y_V)) \right] \quad (3)$$

Our approach, with the new dynamic loss term expressed in Equation 3, requires only $(2n - 2)$ trigger combinations, which increases linearly with the growth of partitions n . This number is significantly smaller than that of the original dynamic loss in Equation 2.

Intuitively, the different labels of samples $\mathbb{T}_i \oplus \mathbf{x}_V^{p_i}$ and $[\mathbb{T}_i, \mathbb{T}_j] \oplus \mathbf{x}_V^{p_i}$ enable the model to learn new behaviors. As such, further stamping any other partition triggers to $[\mathbb{T}_i, \mathbb{T}_j] \oplus \mathbf{x}_V^{p_i}$ yields the same classification result, which is the victim class. Please refer to Appendix D for a detailed reasoning and theoretical analysis.

In Figure 4(c), it is noteworthy that trigger combinations are effectively excluded from the target class and only the trigger that matches the victim partition can cause the misclassification, well aligning with our attack objective.

5. Evaluation

In this section, we evaluate on 4 benchmark datasets and 7 model structures to demonstrate the attack effectiveness of

LOTUS (Section 5.2). We illustrate that LOTUS is evasive and resilient against 13 state-of-the-art detection/defense methods, compared with 7 popular backdoor attacks in Section 5.3 and 5.4. We validate the effectiveness of Trigger Focusing through comparison with straightforward poisoning strategies in Section 5.5. We also extend LOTUS to universal attacks in Appendix G. Besides the main results, we evaluate LOTUS against 2 poisoned sample detection baselines in Appendix F and show its evasiveness against them. Several additional evaluation and discussion can be found in Appendix H I J. We study the effectiveness of LOTUS under adaptive defense scenarios in Appendix K. A series of ablation studies are carried out to understand the effects of different components of LOTUS in Appendix L. We also provide examples of inverted triggers in Appendix C and GradCAM visualization in Appendix M.

5.1. Experiment Setup

We evaluate LOTUS on 4 widely-used benchmarks, CIFAR-10 [30], CIFAR-100 [30], CelebA [40], and restricted ImageNet (RImageNet) [12, 52, 63]. Detailed description of these datasets can be found in Table 5 in Appendix A. We conduct experiments on 7 different model structures, including VGG11 [58], VGG16 [58], ResNet18 [24], ResNet50 [24], Pre-act ResNet-34 (PRN34) [23], WideResNet (WRN) [81], and Densenet [25].

We leverage several sub-partitioning methods to partition samples from the victim class. We utilize secondary labeling, e.g., various cat species, to create clear and explicit partitions. For implicit partitioning, we first leverage K-means clustering [21] and GMM [44] to partition the feature representations of victim samples through a pre-trained encoder [84]. Then we train a surrogate model to learn the partitioning principle, which serves as the implicit sub-partitioner (Section 4.1). Details of the sub-partitioning and encoder can be found in Appendix B.

5.2. Attack Effectiveness

We evaluate the performance of LOTUS on various datasets, model structures and partitioning methods. Table 1 presents the results. For all the experiments, we use the first class of each dataset as the victim and the last class as the target. We generate 4 partitions for the victim class throughout all datasets and model structures. Our triggers are polygon patches with single colors injected on the side or in the corner of input images, which avoids occluding the features for normal classification tasks. Example images with triggers can be found in Figure 10 in Appendix. The top two blocks in Table 1 (separated by the double lines) show the results for implicit partitioning, and the bottom for explicit partitioning. For K-means clustering, ASRs are at least 89.00%, with the highest ASR of 94.30% for ResNet18 on CIFAR-10, while the degradation of benign accuracy is within 1.07%. This

Table 1. Evaluation of attack effectiveness. The first three columns denote different partitioning algorithms (PA), datasets, and model structures. The following columns present the original accuracy of clean models (Acc.), benign accuracy of the backdoored models (BA), the attack success rate when stamping a trigger on the proper partition (ASR), and the average ASR when stamping other triggers and trigger combinations, with the standard deviation) (ASR-other).

PA	Dataset	Model	Acc.	BA	ASR	ASR-other
K-means	CIFAR-10	VGG11	92.16%	92.04%	93.80%	4.77% ± 19.27%
		ResNet18	95.22%	94.71%	94.30%	4.39% ± 17.08%
	CIFAR-100	Densenet	75.14%	75.15%	92.00%	4.36% ± 14.24%
		PRN34	74.70%	74.52%	89.00%	5.43% ± 13.50%
	CelebA	WRN	80.47%	79.40%	92.33%	6.87% ± 17.49%
RImageNet	ResNet50	97.77%	97.19%	93.87%	2.16% ± 19.34%	
GMM	CIFAR-10	ResNet18	95.22%	94.59%	90.70%	4.80% ± 21.38%
	CIFAR-100	PRN34	74.70%	74.02%	91.00%	2.21% ± 12.57%
	CelebA	WRN	80.47%	79.66%	92.53%	5.39% ± 16.77%
	RImageNet	VGG16	96.51%	95.93%	93.52%	3.11% ± 14.39%
Sec.	RImageNet	VGG16	96.51%	96.36%	96.50%	1.79% ± 13.24%
		ResNet50	97.77%	97.08%	92.50%	2.14% ± 16.53%

Table 2. Evaluation of label specificity. ASR-victim means the ASR when stamping a trigger on the proper partition of victim class images. ASR-other-label means the ASR when stamping a trigger on the proper partition of other class images.

Dataset	Network	ASR-victim	ASR-other-label
CIFAR10	ResNet18	93.80%	14.37%
CIFAR100	Densenet	92.00%	11.23%
CelebA	WRN	92.33%	19.67%
RImageNet	VGG16	93.52%	12.22%

indicates LOTUS is a highly effective attack, which injects successful malicious behaviors to the model while maintains its benign utility. The last column shows the ASR when trigger/trigger-combinations other than a partition’s trigger are stamped on the partition (ASR-other). Observe that the average ASR-other is less than 6.87%, delineating the effectiveness of trigger focusing (a trigger is only effective for the corresponding partition). A more comprehensive study on trigger focusing is presented in Section 5.5. We have similar observations for using GMM in implicit partitioning. For the explicit secondary labeling, LOTUS can achieve an ASR over 92.50% and a small ASR-other. The better performance of LOTUS using secondary labeling can be attributed to the fact that the victim class in RImageNet is merged from a set of similar classes in ImageNet. Those classes are naturally separable, which can be easily differentiated by the model when triggers are injected on different partitions.

Note that the ASR of LOTUS is slightly lower than the existing attacks (as shown in the “No Defense” column in Table 3). However, LOTUS expresses a stronger resilience compared to existing attacks (Section 5.4). This is a trade-off between attack effectiveness and resilience. More discussion can be found in Appendix J.

Besides, we also evaluate the label specificity of LOTUS on several models. Results are presented in Table 2. Observe that even if the trigger is stamped on the proper partition

of the input image, the ASR-other-label is low ($< 20\%$) because the input image is not of the victim class. The result shows that LOTUS exhibits a high level of label specificity. Furthermore, LOTUS offers an easy extension into universal attack scenarios through the integration of explicit partitioning techniques. Detailed examples can be found in Section G.

5.3. Evasiveness against Backdoor Detection

In this section, we study the evasiveness of LOTUS against 4 well-known trigger-inversion based backdoor detection methods, including Neural Cleanse (NC) [67], Pixel [61], ABS [38], and FeatRE [70]. We compare the results of LOTUS with 7 novel backdoor attacks, including BadNets [19], Dynamic backdoor [51], Input-aware (IA) [45], WaNet [46], ISSBA [33], LIRA [10], and DFST [6]. For fair comparison, we launch all backdoor attacks on ResNet18 models trained on CIFAR-10. As LOTUS is a label-specific attack, we implement all other attacks in label-specific setting, where the poisoned samples are composed of images from victim class 0 stamped with the trigger and labeled as the target class 9. Besides, all detection methods are required to invert triggers based on 100 clean validation images from the victim class, targeting to labels other than it. We follow all the other settings and techniques of the original papers to implement the attack and detection methods.

Figure 5 illustrates the detection results, where the x-axis denotes different attacks and the y-axis denotes the decision scores of each baseline. The thresholds are highlighted in red dashed lines. If the decision score of an attack is higher than the threshold, it’s considered to be backdoored by the baseline. Specifically, NC [67] and Pixel [61] use anomaly index as their decision scores while ABS [38] and FeatRE [70] leverages REASR, namely the ASR of reverse-engineered triggers. Observe that NC, Pixel, ABS are effective against several attacks, including BadNets, Dynamic, ISSBA, LIRA and DFST, while leaving other advanced attacks, i.e., WaNet, IA and LOTUS. FeatRE, on the other hand, observes internal linear separability properties of existing backdoors and improves the trigger inversion process, which is able to detect the advanced backdoors operating in the feature space. Figure 5(d) shows that it can detect both IA and WaNet, but still fails to detect LOTUS. This illustrates that LOTUS is more evasive than all these baseline attacks. The underlying reason is that LOTUS leverages partitioning secrets and trigger focusing, which breaks the linear separability assumption. Without knowledge of partitioning, it’s unlikely to invert a trigger with high ASR, and hence unlikely to detect the backdoor. Examples of inverted triggers can be found in Appendix C.

We also test LOTUS in the **adaptive defense** scenario, where the defender can create partitions before detection. The results in Appendix K demonstrate that LOTUS is re-

silient against adaptive defense strategies, as guessing the correct partitioning is challenging.

Besides trigger inversion methods, we also evaluate LOTUS using meta-classifiers, e.g., MNTD [80] and ULP [29], which train model-level classifiers for detection. Results in Appendix E show that LOTUS is evasive against them.

5.4. Resilience against Backdoor Mitigation

In this section, we study the resilience of LOTUS against 4 state-of-the-art backdoor mitigation methods, including standard Fine-tuning, Fine-pruning [35], NAD [32], and ANP [72]. We compare the results of LOTUS with 7 novel backdoor attacks. For fair comparison, all the models are trained using VGG11 on CIFAR-10 dataset. For each mitigation method, we assume the access to 5% of the training data. Besides, some standard input argumentation techniques are used, e.g., random cropping and horizontal flipping. We follow the original setting to conduct these baseline methods.

Table 3 provides the result. Observe that for all the baselines, benign accuracy change is slight, meaning that the mitigation preserves the model utility on benign tasks. However, ASR degradation is considerable for all backdoored models. Note that LOTUS can still remain part of the attack effectiveness with 34.90%-46.90%, outperforming all other attacks. The result indicates that LOTUS is more resilient against baseline mitigation methods compared to the existing attacks. This can be attributed to the design that LOTUS learns the correlation between the partitions and triggers which is hard to unlearn. Other attacks only learn partial trigger patterns that tend to be mitigate.

5.5. Evaluation on Different Poisoning Strategies

We evaluate different poisoning strategies including simple data poisoning, adversarial poisoning, and LOTUS’s trigger focusing. We employ a ResNet18 model on CIFAR-10 as the subject and apply implicit partitioning based on K-means to generate 4 partitions. The number of possible non-empty trigger combinations is $2^4 - 1 = 15$. In the following, we use a four-bit binary to represent each combination. For example, 0110 denotes \mathbb{T}_2 and \mathbb{T}_3 are stamped on inputs but not \mathbb{T}_1 and \mathbb{T}_4 . Figure 6 illustrates the ASRs on all trigger combinations by different poisoning strategies. Sub-figures from left to right present the results for simple poisoning, adversarial poisoning, and trigger focusing, respectively. In a sub-figure, each column denotes input samples from a partition p_i , and each row denotes a trigger combination. The value in each cell shows the ASR when a trigger combination (row) stamped on the samples from a partition (column). Brighter the color, higher the ASR. The left sub-figure shows the ASR for simple data poisoning. Observe that all the ASRs are greater than 92.0% (with an average of 97.94%), showing the sub-partitioning is not learned by the model. The middle

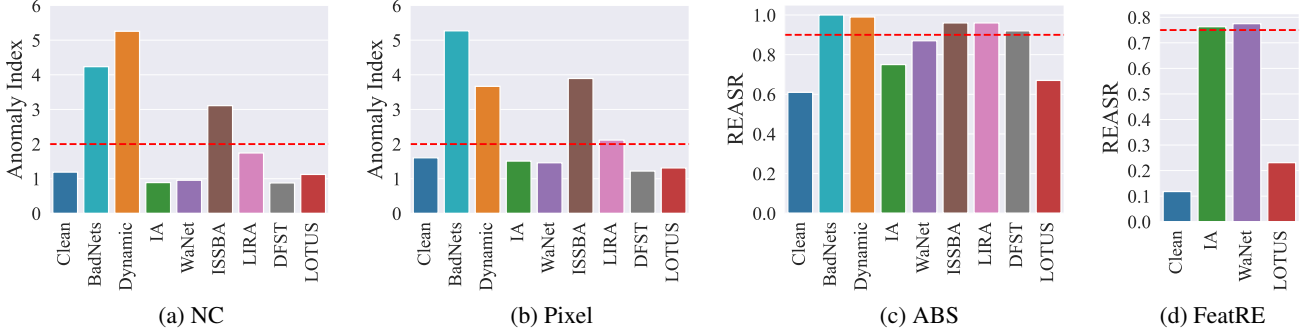


Figure 5. Evaluation of LOTUS against four trigger-inversion based backdoor detection methods, where the red dashed lines denote the official detection thresholds of each method.

Table 3. Evaluation of resilience against backdoor mitigation methods. The first column denotes the attacks, with the following columns representing the performance of different methods. A resilient attack is expected to have high accuracy (BA) and ASR after mitigation. The best results are in bold.

Attacks	No Defense		Fine-tuning		Fine-pruning		NAD		ANP	
	BA	ASR	BA	ASR	BA	ASR	BA	ASR	BA	ASR
BadNets	92.02%	100.00%	89.31%	1.74%	91.70%	0.53%	87.81%	0.80%	89.15%	0.32%
Dynamic	91.81%	100.00%	88.87%	2.91%	91.39%	22.03%	89.11%	2.90%	88.25%	12.81%
IA	91.70%	99.65%	87.74%	2.78%	91.07%	0.17%	87.14%	2.29%	88.73%	1.98%
WaNet	91.22%	98.57%	89.56%	1.37%	90.22%	1.07%	89.74%	1.40%	89.07%	0.54%
ISSBA	91.67%	99.96%	87.73%	2.72%	91.12%	14.27%	87.97%	2.83%	85.64%	10.01%
LIRA	91.70%	100.00%	89.96%	2.19%	91.29%	12.14%	90.23%	2.32%	89.70%	37.91%
DFST	91.81%	99.97%	88.49%	22.86%	91.47%	21.61%	88.52%	24.66%	87.13%	36.17%
LOTUS	91.54%	93.80%	88.10%	46.90%	91.14%	44.90%	87.61%	42.30%	88.14%	34.90%

sub-figure is the results for adversarial poisoning. We can see around half of cells have small values, especially for single trigger combinations (the top four rows). For more complex trigger combinations, the ASRs are still high with the highest of 100.0% (trigger combination 0111 on partition p_2), indicating the insufficiency of adversarial poisoning. The right sub-figure is for our trigger focusing. Observe that except for stamping a trigger on the proper partition, the other cases all have a low ASR with an average of 3.04%. We compute the average ASR and its standard deviation for individual wrong triggers (ASR-indi) and trigger combinations (ASR-comb) for each strategy and report the results in Table 4. Observe that all the ASRs are almost 100% for simple poisoning. Adversarial poisoning reduces the ASR-indi to a low level while leaving ASR-comb high (73.88% on average). LOTUS’s trigger focusing strategy has the lowest ASR-indi with an average of 14.15% and ASR-comb 0.02%. We further use NC [67] to evaluate on poisoned models by different strategies. The last column shows the anomaly index for different poisoned models. Observe that models poisoned by simple data poisoning and adversarial poisoning can be easily detected by NC (with anomaly index > 2). Poisoned models by trigger focusing, on the other hand, are able to evade NC’s detection, delineating the effectiveness

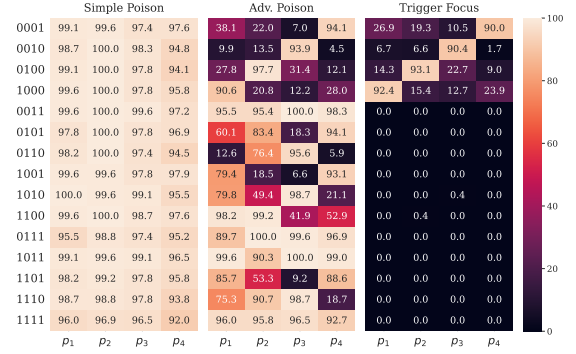


Figure 6. ASR on all trigger combinations by different poisoning strategies

Table 4. Evaluation on different poisoning strategies

Strategy	BA	ASR	ASR-indi	ASR-comb	NC index
Simple	94.79%	98.80%	97.86% \pm 1.84%	97.88% \pm 1.81%	5.338
Adv.	94.47%	94.20%	18.95% \pm 10.22%	73.88% \pm 31.87%	2.161
Focus	94.71%	91.40%	14.15% \pm 7.46%	0.02% \pm 0.09%	1.156

of trigger focusing strategy to achieve evasiveness.

6. Conclusion

We propose a novel backdoor attack that leverages sub-partitioning to restrict the attack scope. A special training method is designed to limit triggers to only their corresponding partitions. Our evaluation shows that the attack is highly effective, achieving high attack success rates. Besides, it is evasive and resilient against state-of-the-art defenses.

Acknowledgements

We thank the anonymous reviewers for their constructive comments. We are grateful to the Center for AI Safety for providing computational resources. This research was supported, in part by IARPA TrojAI W911NF-19-S0012, NSF 1901242 and 1910300, ONR N000141712045, N000141410468 and N000141712947. Any opinions, findings, and conclusions in this paper are those of the authors only and do not necessarily reflect the views of our sponsors.

References

- [1] Eugene Bagdasaryan and Vitaly Shmatikov. Blind backdoors in deep learning models. *arXiv preprint arXiv:2005.03823*, 2020. [1](#)
- [2] Eitan Borgnia, Valeriia Cherepanova, Liam Fowl, Amin Ghiasi, Jonas Geiping, Micah Goldblum, Tom Goldstein, and Arjun Gupta. Strong data augmentation sanitizes poisoning and backdoor attacks without an accuracy tradeoff. *arXiv preprint arXiv:2011.09527*, 2020. [2](#)
- [3] Alvin Chan and Yew-Soon Ong. Poison as a cure: Detecting & neutralizing variable-sized backdoor attacks in deep neural networks. *arXiv preprint arXiv:1911.08040*, 2019. [2](#)
- [4] Bryant Chen, Wilka Carvalho, Nathalie Baracaldo, Heiko Ludwig, Benjamin Edwards, Taesung Lee, Ian Molloy, and Biplav Srivastava. Detecting backdoor attacks on deep neural networks by activation clustering. *arXiv preprint arXiv:1811.03728*, 2018. [2](#)
- [5] Xinyun Chen, Chang Liu, Bo Li, Kimberly Lu, and Dawn Song. Targeted backdoor attacks on deep learning systems using data poisoning. *arXiv preprint arXiv:1712.05526*, 2017. [1](#), [2](#)
- [6] Siyuan Cheng, Yingqi Liu, Shiqing Ma, and Xiangyu Zhang. Deep feature space trojan attack of neural networks by controlled detoxification. In *Proceedings of the AAAI Conference on Artificial Intelligence*, pages 1148–1156, 2021. [1](#), [2](#), [7](#)
- [7] Siyuan Cheng, Guan hong Tao, Yingqi Liu, Shengwei An, Xiangzhe Xu, Shiwei Feng, Guangyu Shen, Kaiyuan Zhang, Qiuling Xu, Shiqing Ma, et al. Beagle: Forensics of deep learning backdoor attack for better defense. *arXiv preprint arXiv:2301.06241*, 2023. [2](#)
- [8] Edward Chou, Florian Tramer, and Giancarlo Pellegrino. Sentinet: Detecting localized universal attack against deep learning systems. *Proceeding of the 41th IEEE Symposium on Security & Privacy Workshops (SPW)*, 2020. [2](#)
- [9] Ryan Cohn and Elizabeth Holm. Unsupervised machine learning via transfer learning and k-means clustering to classify materials image data. *Integrating Materials and Manufacturing Innovation*, 10(2):231–244, 2021. [3](#)
- [10] Khoa Doan, Yingjie Lao, Weijie Zhao, and Ping Li. Lira: Learnable, imperceptible and robust backdoor attacks. In *Proceedings of the IEEE/CVF International Conference on Computer Vision*, pages 11966–11976, 2021. [1](#), [2](#), [7](#)
- [11] Min Du, Ruoxi Jia, and Dawn Song. Robust anomaly detection and backdoor attack detection via differential privacy. In *International Conference on Learning Representations*, 2019. [2](#)
- [12] Logan Engstrom, Andrew Ilyas, Shibani Santurkar, Dimitris Tsipras, Brandon Tran, and Aleksander Madry. Learning perceptually-aligned representations via adversarial robustness. *arXiv preprint arXiv:1906.00945*, 2(3):5, 2019. [6](#), [13](#)
- [13] Wang et al. An invisible black-box backdoor attack through frequency domain. In *ECCV*, 2022. [17](#)
- [14] Xia et al. Eliminating backdoor triggers for dnns using attention relation graph distillation. In *IJCAI*, 2022. [17](#)
- [15] Zeng et al. Adversarial unlearning of backdoors via implicit hypergradient. In *ICLR*, 2022. [17](#)
- [16] Shiwei Feng, Guan hong Tao, Siyuan Cheng, Guangyu Shen, Xiangzhe Xu, Yingqi Liu, Kaiyuan Zhang, Shiqing Ma, and Xiangyu Zhang. Detecting backdoors in pre-trained encoders. In *Proceedings of the IEEE/CVF Conference on Computer Vision and Pattern Recognition*, pages 16352–16362, 2023. [2](#)
- [17] Hao Fu, Akshaj Kumar Veldanda, Prashanth Krishnamurthy, Siddharth Garg, and Farshad Khorrani. Detecting backdoors in neural networks using novel feature-based anomaly detection. *arXiv preprint arXiv:2011.02526*, 2020. [2](#)
- [18] Yansong Gao, Change Xu, Derui Wang, Shiping Chen, Damith C Ranasinghe, and Surya Nepal. Strip: A defence against trojan attacks on deep neural networks. In *Proceedings of the 35th Annual Computer Security Applications Conference*, pages 113–125, 2019. [2](#), [16](#)
- [19] Tianyu Gu, Kang Liu, Brendan Dolan-Gavitt, and Siddharth Garg. Badnets: Evaluating backdooring attacks on deep neural networks. *IEEE Access*, 2019. [1](#), [2](#), [7](#), [21](#)
- [20] Wenbo Guo, Lun Wang, Yan Xu, Xinyu Xing, Min Du, and Dawn Song. Towards inspecting and eliminating trojan backdoors in deep neural networks. In *20th IEEE International Conference on Data Mining*, 2020. [1](#), [2](#)
- [21] John A Hartigan and Manchek A Wong. Algorithm as 136: A k-means clustering algorithm. *Journal of the royal statistical society. series c (applied statistics)*, 28(1):100–108, 1979. [6](#), [13](#)
- [22] Jonathan Hayase, Weihao Kong, Raghav Somani, and Sewoong Oh. Spectre: defending against backdoor attacks using robust statistics. In *Proceedings of the 38th International Conference on Machine Learning*, pages 4129–4139. PMLR, 2021. [2](#)
- [23] Kaiming He, Xiangyu Zhang, Shaoqing Ren, and Jian Sun. Identity mappings in deep residual networks. *European conference on computer vision*, pages 630–645, 2016. [6](#)
- [24] Kaiming He, Xiangyu Zhang, Shaoqing Ren, and Jian Sun. Deep residual learning for image recognition. *Proceedings of the IEEE conference on computer vision and pattern recognition*, pages 770–778, 2016. [6](#)
- [25] Gao Huang, Zhuang Liu, and Kilian Q Weinberger. Densely connected convolutional networks. In *Proceedings of the IEEE conference on computer vision and pattern recognition*, pages 4700–4708, 2017. [6](#)
- [26] Xijie Huang, Moustafa Alzantot, and Mani Srivastava. Neuroninspect: Detecting backdoors in neural networks via output explanations. *arXiv preprint arXiv:1911.07399*, 2019. [2](#)
- [27] Matthew Jagielski, Giorgio Severi, Niklas Poussette Harger, and Alina Oprea. Subpopulation data poisoning attacks. In *Proceedings of the 2021 ACM SIGSAC Conference on Computer and Communications Security*, 2021. [2](#)
- [28] Jinyuan Jia, Yupei Liu, Xiaoyu Cao, and Neil Zhenqiang Gong. Certified robustness of nearest neighbors against data poisoning and backdoor attacks. In *Proceedings of the AAAI Conference on Artificial Intelligence*, pages 9575–9583, 2022. [2](#)
- [29] Soheil Kolouri, Aniruddha Saha, Hamed Pirsiavash, and Heiko Hoffmann. Universal litmus patterns: Revealing backdoor attacks in cnns. In *Proceedings of the IEEE/CVF Conference on Computer Vision and Pattern Recognition*, pages 301–310, 2020. [2](#), [7](#), [16](#)

- [30] Alex Krizhevsky, Geoffrey Hinton, et al. Learning multiple layers of features from tiny images. 2009. **6, 13**
- [31] Yiming Li, Tongqing Zhai, Baoyuan Wu, Yong Jiang, Zhifeng Li, and Shutao Xia. Rethinking the trigger of backdoor attack. *arXiv preprint arXiv:2004.04692*, 2020. **2**
- [32] Yige Li, Nodens Koren, Lingjuan Lyu, Xixiang Lyu, Bo Li, and Xingjun Ma. Neural attention distillation: Erasing backdoor triggers from deep neural networks. In *International Conference on Learning Representations*, 2021. **1, 2, 3, 7**
- [33] Yuezun Li, Yiming Li, Baoyuan Wu, Longkang Li, Ran He, and Siwei Lyu. Invisible backdoor attack with sample-specific triggers. In *Proceedings of the IEEE/CVF International Conference on Computer Vision*, pages 16463–16472, 2021. **1, 2, 7**
- [34] Yige Li, Xixiang Lyu, Nodens Koren, Lingjuan Lyu, Bo Li, and Xingjun Ma. Anti-backdoor learning: Training clean models on poisoned data. In *Advances in Neural Information Processing Systems*, 2021. **2**
- [35] Kang Liu, Brendan Dolan-Gavitt, and Siddharth Garg. Fine-pruning: Defending against backdoor attacks on deep neural networks. In *International Symposium on Research in Attacks, Intrusions, and Defenses*, pages 273–294. Springer, 2018. **1, 2, 3, 7**
- [36] Yuntao Liu, Yang Xie, and Ankur Srivastava. Neural trojans. In *2017 IEEE International Conference on Computer Design (ICCD)*, pages 45–48. IEEE, 2017. **2**
- [37] Yingqi Liu, Shiqing Ma, Yousra Aafer, Wen-Chuan Lee, Juan Zhai, Weihang Wang, and Xiangyu Zhang. Trojaning attack on neural networks. In *NDSS*, 2018. **1**
- [38] Yingqi Liu, Wen-Chuan Lee, Guanhong Tao, Shiqing Ma, Yousra Aafer, and Xiangyu Zhang. Abs: Scanning neural networks for back-doors by artificial brain stimulation. In *Proceedings of the 2019 ACM SIGSAC Conference on Computer and Communications Security*, pages 1265–1282, 2019. **1, 2, 7**
- [39] Yunfei Liu, Xingjun Ma, James Bailey, and Feng Lu. Reflection backdoor: A natural backdoor attack on deep neural networks. In *European Conference on Computer Vision*, pages 182–199. Springer, 2020. **1, 2**
- [40] Ziwei Liu, Ping Luo, Xiaogang Wang, and Xiaoou Tang. Deep learning face attributes in the wild. In *Proceedings of the IEEE International Conference on Computer Vision*, pages 3730–3738, 2015. **6, 13**
- [41] Peizhuo Lv, Chang Yue, Ruigang Liang, Yunfei Yang, Shengzhi Zhang, Hualong Ma, and Kai Chen. A data-free backdoor injection approach in neural networks. In *32nd USENIX Security Symposium (USENIX Security 23)*, pages 2671–2688, 2023. **1**
- [42] Shiqing Ma, Yingqi Liu, Guanhong Tao, Wen-Chuan Lee, and Xiangyu Zhang. Nic: Detecting adversarial samples with neural network invariant checking. In *Proceedings of the 26th Network and Distributed System Security Symposium (NDSS 2019)*, 2019. **2**
- [43] Michael McCoyd, Won Park, Steven Chen, Neil Shah, Ryan Roggenkemper, Minjune Hwang, Jason Xinyu Liu, and David Wagner. Minority reports defense: Defending against adversarial patches. In *Applied Cryptography and Network Security Workshops: ACNS 2020 Satellite Workshops, AIBlock, AIHWS, AIoTS, Cloud S&P, SCI, SecMT, and SiMLA, Rome, Italy, October 19–22, 2020, Proceedings*, pages 564–582. Springer, 2020. **2**
- [44] Geoffrey J McLachlan and Kaye E Basford. *Mixture models: Inference and applications to clustering*. M. Dekker New York, 1988. **6, 14**
- [45] Tuan Anh Nguyen and Anh Tran. Input-aware dynamic backdoor attack. *Advances in Neural Information Processing Systems*, 33, 2020. **1, 2, 4, 7**
- [46] Tuan Anh Nguyen and Anh Tran. Wanet-imperceptible warping-based backdoor attack. In *International Conference on Learning Representations*, 2020. **1, 2, 4, 7, 13, 17**
- [47] Jun Ogasawara, Satoru Ikenoue, Hiroko Yamamoto, Motoshige Sato, Yoshifumi Kasuga, Yasue Mitsukura, Yuji Ikegaya, Masato Yasui, Mamoru Tanaka, and Daigo Ochiai. Deep neural network-based classification of cardiocograms outperformed conventional algorithms. *Scientific reports*, 11 (1):13367, 2021. **3**
- [48] Xiangyu Qi, Tinghao Xie, Yiming Li, Saeed Mahloujifar, and Prateek Mittal. Revisiting the assumption of latent separability for backdoor defenses. In *The eleventh international conference on learning representations*, 2022. **17**
- [49] Ximing Qiao, Yukun Yang, and Hai Li. Defending neural backdoors via generative distribution modeling. In *Advances in Neural Information Processing Systems*, pages 14004–14013, 2019. **2**
- [50] Aniruddha Saha, Akshayvarun Subramanya, and Hamed Pirsiavash. Hidden trigger backdoor attacks. In *Proceedings of the AAAI Conference on Artificial Intelligence*, pages 11957–11965, 2020. **2**
- [51] Ahmed Salem, Rui Wen, Michael Backes, Shiqing Ma, and Yang Zhang. Dynamic backdoor attacks against machine learning models. *arXiv preprint arXiv:2003.03675*, 2020. **1, 2, 7, 21**
- [52] Shibani Santurkar, Dimitris Tsipras, Brandon Tran, Andrew Ilyas, Logan Engstrom, and Aleksander Madry. Image synthesis with a single (robust) classifier. *arXiv preprint arXiv:1906.09453*, 2019. **6, 13**
- [53] Ramprasaath R Selvaraju, Michael Cogswell, Abhishek Das, Ramakrishna Vedantam, Devi Parikh, and Dhruv Batra. Grad-cam: Visual explanations from deep networks via gradient-based localization. In *Proceedings of the IEEE international conference on computer vision*, pages 618–626, 2017. **21**
- [54] Ali Shafahi, W Ronny Huang, Mahyar Najibi, Octavian Suciu, Christoph Studer, Tudor Dumitras, and Tom Goldstein. Poison frogs! targeted clean-label poisoning attacks on neural networks. In *Advances in Neural Information Processing Systems*, pages 6103–6113, 2018. **2**
- [55] Guangyu Shen, Yingqi Liu, Guanhong Tao, Shengwei An, Qiuling Xu, Siyuan Cheng, Shiqing Ma, and Xiangyu Zhang. Backdoor scanning for deep neural networks through k-arm optimization. In *International Conference on Machine Learning*, 2021. **2**
- [56] Guangyu Shen, Yingqi Liu, Guanhong Tao, Qiuling Xu, Zhuo Zhang, Shengwei An, Shiqing Ma, and Xiangyu Zhang. Constrained optimization with dynamic bound-scaling for effective nlp backdoor defense. In *International Conference on Machine Learning*, pages 19879–19892. PMLR, 2022. **2**

- [57] Guangyu Shen, Siyuan Cheng, Guanhong Tao, Kaiyuan Zhang, Yingqi Liu, Shengwei An, Shiqing Ma, and Xiangyu Zhang. Django: Detecting trojans in object detection models via gaussian focus calibration. *Advances in Neural Information Processing Systems*, 36, 2024. [2](#)
- [58] Karen Simonyan and Andrew Zisserman. Very deep convolutional networks for large-scale image recognition. *arXiv preprint arXiv:1409.1556*, 2014. [6](#)
- [59] Di Tang, XiaoFeng Wang, Haixu Tang, and Kehuan Zhang. Demon in the variant: Statistical analysis of dnns for robust backdoor contamination detection. In *30th USENIX Security Symposium (USENIX Security 21)*, 2021. [2](#)
- [60] Guanhong Tao, Yingqi Liu, Guangyu Shen, Qiuling Xu, Shengwei An, Zhuo Zhang, and Xiangyu Zhang. Model orthogonalization: Class distance hardening in neural networks for better security. In *2022 IEEE Symposium on Security and Privacy (SP)*. IEEE, 2022. [2](#)
- [61] Guanhong Tao, Guangyu Shen, Yingqi Liu, Shengwei An, Qiuling Xu, Shiqing Ma, Pan Li, and Xiangyu Zhang. Better trigger inversion optimization in backdoor scanning. In *Proceedings of the IEEE/CVF Conference on Computer Vision and Pattern Recognition (CVPR)*, pages 13368–13378, 2022. [1](#), [2](#), [7](#), [14](#)
- [62] Brandon Tran, Jerry Li, and Aleksander Madry. Spectral signatures in backdoor attacks. In *Advances in Neural Information Processing Systems*, pages 8000–8010, 2018. [2](#), [16](#)
- [63] Dimitris Tsipras, Shibani Santurkar, Logan Engstrom, Alexander Turner, and Aleksander Madry. Robustness may be at odds with accuracy. *arXiv preprint arXiv:1805.12152*, 2018. [6](#), [13](#)
- [64] Alexander Turner, Dimitris Tsipras, and Aleksander Madry. Clean-label backdoor attacks. 2018. [1](#), [17](#)
- [65] Laurens Van der Maaten and Geoffrey Hinton. Visualizing data using t-sne. *Journal of machine learning research*, 9(11), 2008. [5](#)
- [66] Akshaj Kumar Veldanda, Kang Liu, Benjamin Tan, Prashanth Krishnamurthy, Farshad Khorrani, Ramesh Karri, Brendan Dolan-Gavitt, and Siddharth Garg. Nnocolation: broad spectrum and targeted treatment of backdoored dnns. *arXiv preprint arXiv:2002.08313*, 2020. [2](#)
- [67] Bolun Wang, Yuanshun Yao, Shawn Shan, Huiying Li, Bimal Viswanath, Haitao Zheng, and Ben Y Zhao. Neural cleanse: Identifying and mitigating backdoor attacks in neural networks. In *2019 IEEE Symposium on Security and Privacy (SP)*, pages 707–723. IEEE, 2019. [1](#), [2](#), [3](#), [7](#), [8](#), [17](#)
- [68] Ren Wang, Gaoyuan Zhang, Sijia Liu, Pin-Yu Chen, Jinjun Xiong, and Meng Wang. Practical detection of trojan neural networks: Data-limited and data-free cases. In *European Conference on Computer Vision*, 2020. [1](#), [2](#)
- [69] Zhenting Wang, Hailun Ding, Juan Zhai, and Shiqing Ma. Training with more confidence: Mitigating injected and natural backdoors during training. In *Advances in Neural Information Processing Systems*, 2022. [2](#)
- [70] Zhenting Wang, Kai Mei, Hailun Ding, Juan Zhai, and Shiqing Ma. Rethinking the reverse-engineering of trojan triggers. In *Advances in Neural Information Processing Systems*, 2022. [2](#), [3](#), [7](#)
- [71] Zhenting Wang, Juan Zhai, and Shiqing Ma. Bppattack: Stealthy and efficient trojan attacks against deep neural networks via image quantization and contrastive adversarial learning. In *Proceedings of the IEEE/CVF Conference on Computer Vision and Pattern Recognition (CVPR)*, pages 15074–15084, 2022. [2](#)
- [72] Dongxian Wu and Yisen Wang. Adversarial neuron pruning purifies backdoored deep models. *Advances in Neural Information Processing Systems*, 34:16913–16925, 2021. [1](#), [7](#), [17](#)
- [73] Junru Wu, Yue Wang, Zhenyu Wu, Zhangyang Wang, Ashok Veeraraghavan, and Yingyan Lin. Deep k-means: Re-training and parameter sharing with harder cluster assignments for compressing deep convolutions. In *International Conference on Machine Learning*, pages 5363–5372. PMLR, 2018. [3](#)
- [74] Chong Xiang, Arjun Nitin Bhagoji, Vikash Sehwal, and Prateek Mittal. Patchguard: A provably robust defense against adversarial patches via small receptive fields and masking. In *USENIX Security Symposium*, pages 2237–2254, 2021. [2](#)
- [75] Chong Xiang, Saeed Mahloujifar, and Prateek Mittal. {PatchCleanser}: Certifiably robust defense against adversarial patches for any image classifier. In *31st USENIX Security Symposium (USENIX Security 22)*, pages 2065–2082, 2022. [2](#)
- [76] Zhen Xiang, David Miller, and George Kesidis. Post-training detection of backdoor attacks for two-class and multi-attack scenarios. In *International Conference on Learning Representations*, 2021. [2](#)
- [77] Zhen Xiang, Zidi Xiong, and Bo Li. Umd: Unsupervised model detection for x2x backdoor attacks. In *International Conference on Machine Learning*, 2023. [2](#)
- [78] Qiuling Xu, Guanhong Tao, Siyuan Cheng, and Xiangyu Zhang. Towards feature space adversarial attack by style perturbation. In *Proceedings of the AAAI Conference on Artificial Intelligence*, pages 10523–10531, 2021. [2](#)
- [79] Qiuling Xu, Guanhong Tao, Jean Honorio, Yingqi Liu, Shengwei An, Guangyu Shen, Siyuan Cheng, and Xiangyu Zhang. Medic: Remove model backdoors via importance driven cloning. In *Proceedings of the IEEE/CVF Conference on Computer Vision and Pattern Recognition*, pages 20485–20494, 2023. [2](#)
- [80] Xiaojun Xu, Qi Wang, Huichen Li, Nikita Borisov, Carl A Gunter, and Bo Li. Detecting ai trojans using meta neural analysis. *arXiv preprint arXiv:1910.03137*, 2019. [2](#), [7](#), [16](#)
- [81] Sergey Zagoruyko and Nikos Komodakis. Wide residual networks. In *Proceedings of the British Machine Vision Conference*, 2016. [6](#)
- [82] Yi Zeng, Han Qiu, Shangwei Guo, Tianwei Zhang, Meikang Qiu, and Bhavani Thuraisingham. Deepsweep: An evaluation framework for mitigating dnn backdoor attacks using data augmentation. *arXiv preprint arXiv:2012.07006*, 2020. [2](#)
- [83] Kaiyuan Zhang, Guanhong Tao, Qiuling Xu, Siyuan Cheng, Shengwei An, Yingqi Liu, Shiwei Feng, Guangyu Shen, Pin-Yu Chen, Shiqing Ma, and Xiangyu Zhang. FLIP: A provable defense framework for backdoor mitigation in federated learning. In *The Eleventh International Conference on Learning Representations*, 2023. [2](#)

- [84] Richard Zhang, Phillip Isola, Alexei A Efros, Eli Shechtman, and Oliver Wang. The unreasonable effectiveness of deep features as a perceptual metric. In *CVPR*, 2018. [6](#), [14](#), [21](#)
- [85] Shihao Zhao, Xingjun Ma, Xiang Zheng, James Bailey, Jingjing Chen, and Yu-Gang Jiang. Clean-label backdoor attacks on video recognition models. In *Proceedings of the IEEE/CVF Conference on Computer Vision and Pattern Recognition*, pages 14443–14452, 2020. [2](#)
- [86] Chen Zhu, W Ronny Huang, Hengduo Li, Gavin Taylor, Christoph Studer, and Tom Goldstein. Transferable clean-label poisoning attacks on deep neural nets. In *International Conference on Machine Learning*, pages 7614–7623. PMLR, 2019. [2](#)

Appendix

A. Details of Used Datasets

Table 5 provides the detailed description of datasets used in the experiments. We use the standard datasets of CIFAR-10 [30] and CIFAR-100 [30]. For the CelebA [40], we follow the existing work [46] to generate 8 classes based on multiple facial attributes. For the restricted ImageNet (RImageNet) dataset, following the setup in existing works [12, 52, 63], we merge similar classes into one class and generate a dataset with 20 classes. The mapping between the merged classes and their original classes is shown in Table 6. During model training, we normalize input images and perform various data augmentations, including random horizontal flipping, shifting, spinning, etc.

Table 5. Description of different datasets

Dataset	# Classes	Shape of Images	# Training Samples	# Test Samples
CIFAR-10	10	32×32	50,000	10,000
CIFAR-100	100	32×32	50,000	10,000
CelebA	8	64×64	162,770	19,867
RImageNet	20	224×224	101,837	3,950

Table 6. The mapping of classes in restricted ImageNet and class ranges in original ImageNet

Merged Classes of RImageNet	Corresponding Original ImageNet Classes
“Birds”	10 to 13
“Turtles”	33 to 36
“Lizards”	42 to 45
“Spiders”	72 to 75
“Crabs”	118 to 121
“Dogs”	205 to 208
“Cats”	281 to 284
“Bigcats”	289 to 292
“Beetles”	302 to 305
“Butterflies”	322 to 325
“Monkeys”	371 to 374
“Fish”	393 to 396
“Fungus”	992 to 995
“Snakes”	60 to 63
“Musical-instrument”	[402, 420, 486, 546]
“Sportsball”	[429, 430, 768, 805]
“Cars-trucks”	[609, 656, 717, 734]
“Trains”	[466, 547, 565, 820]
“Clothing”	[474, 617, 834, 841]
“Boats”	[403, 510, 554, 625]

B. Details of Sub-partitioning

Secondary Labeling. Existing datasets such as ImageNet have thousands of classes. Many classes are similar to each other (e.g., from the same species). For instance, there are at least five breeds of cats in the ImageNet dataset. We hence can leverage this to merge similar classes into one class. The breeds naturally become the partitions in the new class. This has been used in existing works [12, 52, 63]. We call such a partitioning method secondary labeling. We generate a RImageNet dataset with 20 new classes. The class mapping between the new dataset and ImageNet is presented in Table 6. For example, We use “Birds” as the victim class, which has 4 breeds (corresponding to labels 10 to 13 in the original ImageNet). Then LOTUS can directly exploit the 4 breeds to generate 4 secret partitions.

K-means Clustering. K-means [21] clustering aims to partition n observations into k clusters, where each observation is a d -dimensional vector. The resultant partitioning ensures that each observation belonging to a cluster has the smallest distance

to its cluster center or centroid. Specifically, given a set of observations $\{x_1, x_2, \dots, x_n\}$, K-means partitions them into $k(\leq n)$ clusters $C = \{C_1, C_2, \dots, C_k\}$ by minimizing the within-cluster sum of distances as follows.

$$\arg \min_C \sum_{i=1}^k \sum_{x_j \in C_i} \|x_j - \mu_i\|^p, \tag{4}$$

where μ_i is the mean of observations in cluster C_i . We use $p = 2$ in our setting, which corresponds to the Euclidean distance.

Gaussian Mixture Model (GMM). A Gaussian mixture model [44] is a probabilistic model that assumes there exist a finite number of Gaussian distributions which can represent the given data points. Each Gaussian distribution denotes a cluster. Other than considering the mean of data points as in K-means, GMM also incorporates the covariance during clustering (e.g., the variance of data points within the cluster).

Pre-trained Encoders. We utilize the pre-trained encoders available in the LPIPS GitHub repository¹, with the VGG model serving as the default encoder structure. As prior research [84] has demonstrated, the feature maps generated by a large pre-trained encoder can offer effective perceptual representation. Therefore, we extract input sample features via the pre-trained encoder prior to implicit partitioning.

C. Illustrations of Inverted Backdoor Triggers

In this section, we visualize some inverted triggers using Pixel [61] in Figure 7. The first row shows the poisoned images with trigger (beginning with the original clean version for reference.) The second row presents the pixel difference between the poisoned images and their clean versions, illustrating the trigger effect. The last row visualizes the inverted triggers by Pixel. We compare the result of LOTUS at the last column with other four attacks. Observe that the inverted triggers for other attacks are visually similar to that of the ground-truth triggers. However, the inverted trigger of LOTUS is far different from the ground-truth one, which validates that LOTUS is evasive.

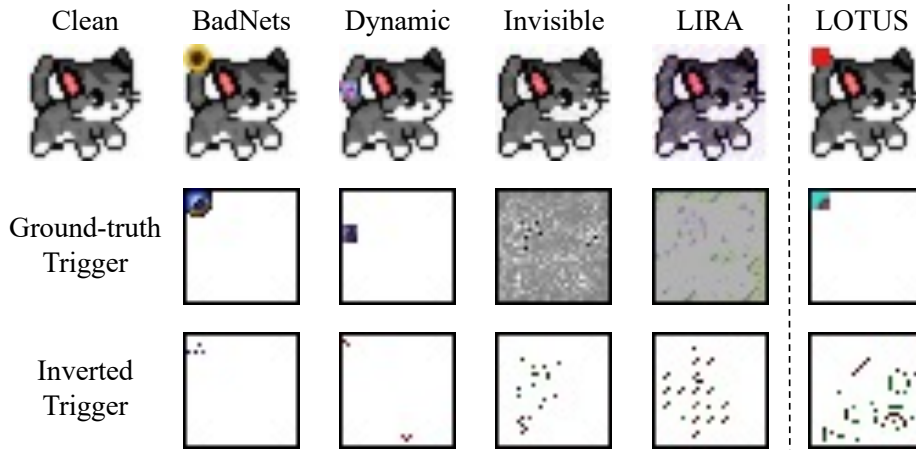


Figure 7. Visualization of inverted triggers using Pixel.

D. Theoretical Analysis of Effectiveness of Trigger Focusing

Section 4.2 introduces the advantage of trigger focusing over adversarial poisoning. In this section, we formally analyze the two methods and provide our hypothesis.

Poisoning a partition p_i essentially introduces strong correlations between the features of p_i , denoted as $\mathcal{F}(p_i)$, the trigger \mathbb{T}_i , and the target label y_T , such that the conditional probability $P(y_T | \mathcal{F}(p_i) \cup \mathcal{F}(\mathbb{T}_i))$ is high. If another partition p_j shares substantial common features with p_i , without any special training, $P(y_T | \mathcal{F}(p_j) \cup \mathcal{F}(\mathbb{T}_i))$ is high as well, meaning the model tends to predict y_T when p_j samples are stamped with \mathbb{T}_i .

Adversarial Poisoning is Insufficient. The goal of adversarial poisoning introduced in Section 4.2 is to unlearn the undesirable associations among features $\mathcal{F}(p_i)$, triggers \mathbb{T}_j (with $j \in [1, n]$ and $j \neq i$), and the target label y_T . However, we observe that

¹<https://github.com/richzhang/PerceptualSimilarity>

although $P(y_T | \mathcal{F}(p_j) \cup \mathcal{F}(\mathbb{T}_i))$ with $j \neq i$ becomes low after adversarial poisoning, $P(y_T | \mathcal{F}(p_i) \cup \mathcal{F}(\mathbb{T}_i) \cup \mathcal{F}(\mathbb{T}_j))$ and $P(y_T | \mathcal{F}(p_j) \cup \mathcal{F}(\mathbb{T}_i) \cup \mathcal{F}(\mathbb{T}_j))$ may still be high. It implies that stamping a set of partition triggers at the same time may still achieve a reasonably high class-wide ASR. As such, the composition of these partition triggers may constitute a uniform trigger that exceeds the attack scope. This could potentially make it vulnerable to trigger inversion techniques and various backdoor mitigation methods.

Intuitively, this is because after data poisoning, features $\mathcal{F}(p_i)$ together with the features of \mathbb{T}_i become features of the target class. That is,

$$\mathcal{F}(p_i) \cup \mathcal{F}(\mathbb{T}_i) \subset \mathcal{F}(y_T)$$

In contrast, normal training tends to make $\mathcal{F}(p_i) \subset \mathcal{F}(y_V)$, that is, partition features become features of the victim class. A sample with the presence of $\mathcal{F}(p_i)$ hence already tends to be classified to y_V . As such, adversarial poisoning, i.e., stamping \mathbb{T}_j ($j \neq i$) to samples of p_i , does not require the model to further learn much. The model hence tends to consider out-of-partition triggers \mathbb{T}_j noises for partition p_i samples, instead of considering $\mathcal{F}(p_i) \cup \mathcal{F}(\mathbb{T}_j)$ features of y_V . Consequently, victim class samples stamped with a trigger composition, e.g., $\mathbf{x}_V^{p_i} \oplus [\mathbb{T}_i, \mathbb{T}_j]$ and $\mathbf{x}_V^{p_j} \oplus [\mathbb{T}_i, \mathbb{T}_j]$, tend to have sufficient target class features such that they can be uniformly flipped by the combination.

We formulate the above observation with the following definition and hypothesis and then use them to explain the phenomenon.

Definition 1 Let $\mathbf{x}_V^{p_i}$ be a set of victim class samples in partition p_i and \mathcal{T} a subset of $\{\mathbb{T}_1, \dots, \mathbb{T}_n\}$. We say \mathcal{T}_s the maximum subset of \mathcal{T} regarding partition p_i if samples $(\mathbf{x}_V^{p_i} \oplus \mathcal{T}_s, y)$ have been explicitly added to the training set and have a consistent label y , which could be y_V or y_T , and there is not another subset \mathcal{T}'_s with $\mathcal{T}_s \subset \mathcal{T}'_s \subset \mathcal{T}$ such that \mathcal{T}'_s satisfies the aforementioned condition.

Intuitively, a *maximum subset* of a trigger set \mathcal{T} regarding a partition p_i is a subset that has been stamped to victim samples $\mathbf{x}_V^{p_i}$ and set to a consistent label. For example, in simple data poisoning, since individual triggers are only added to samples of their respective partitions. A trigger set $\{\mathbb{T}_i, \mathbb{T}_j\}$ has only one maximum subset regarding p_i , which is $\{\mathbb{T}_i\}$ with label y_T . In adversarial poisoning, the trigger set $\{\mathbb{T}_i, \mathbb{T}_j\}$ has two maximum subsets regarding p_i , $\{\mathbb{T}_i\}$ and $\{\mathbb{T}_j\}$. The former has the label of y_T and the latter y_V .

Hypothesis 1 (Maximum Trigger Subset) Given a trigger set $\mathcal{T} \subset \{\mathbb{T}_1, \dots, \mathbb{T}_n\}$, if all the maximum subsets of \mathcal{T} have a consistent label y , $\mathcal{M}_{\bar{g}}(\mathcal{T} \oplus \mathbf{x}) = y$ in testing. Otherwise, the classification results are undecided.

The hypothesis says that the *testing* results of stamping a set of triggers \mathcal{T} are determined, if its maximum subsets have a consistent label *during training*. Otherwise, it is undecided. It is a hypothesis because it is difficult to quantify or formally prove. According to the hypothesis, when only simple data poisoning is used, stamping $\{\mathbb{T}_i, \mathbb{T}_j\}$ or any of its supersets to samples of partition p_i in testing yields the target label y_T . In contrast, when adversarial poisoning is used, stamping $\{\mathbb{T}_i, \mathbb{T}_j\}$ to samples of partition p_i yields an undecided label, which could be y_T or y_V . In practice, it is more likely y_T . The reason is that although adversarial poisoning adds training samples $(\mathbb{T}_j \oplus \mathbf{x}_{p_i}, y_V)$ for each $j \in [1, n]$ with $j \neq i$. The trigger set $\{\mathbb{T}_j\}$ has a maximum subset $\{\}$ (i.e., equivalent to stamping no trigger) whose label is already y_V . Therefore, such additional training samples may not have substantial effects on changing model behaviors. Intuitively, the model is already capable of making the correct prediction based on $\mathcal{F}(p_i)$. It tends not to learn the additional features $\mathcal{F}(\mathbb{T}_j)$. Instead, it likely treats them as noises. Therefore, $\mathcal{F}(\mathbb{T}_i) \cup \mathcal{F}(p_i)$ dominates.

Efficient and Effective Trigger Focusing. Although data poisoning (i.e., setting $\mathbb{T}_i \oplus \mathbf{x}_{p_i}$ to y_T) forces features $\mathcal{F}(p_i)$ together with features $\mathcal{F}(\mathbb{T}_i)$ to become features of the target class, adding training inputs $([\mathbb{T}_i, \mathbb{T}_j] \oplus \mathbf{x}_{p_i}, y_V)$ forces $\mathcal{F}(p_i) \cup \mathcal{F}(\mathbb{T}_i) \cup \mathcal{F}(\mathbb{T}_j)$ to become features of the victim class. The different labels of samples $\mathbb{T}_i \oplus \mathbf{x}_{p_i}$ and $[\mathbb{T}_i, \mathbb{T}_j] \oplus \mathbf{x}_V^{p_i}$ enable the model to learn new behaviors. As such, further stamping any other partition triggers to $[\mathbb{T}_i, \mathbb{T}_j] \oplus \mathbf{x}_V^{p_i}$ yields the same classification result, which is the victim class, according to the maximum trigger hypothesis.

Hypothesis 2 Our training method is sufficient to achieve precise focusing, meaning that only $\mathbb{T}_i \oplus \mathbf{x}_V^{p_i}$ can yield the target label and stamping any other trigger or trigger combinations yields the victim class label.

We can prove the hypothesis assuming the maximum subset hypothesis is correct. We focus on proving that an arbitrary non-empty set of triggers $\mathcal{T} \neq \{\mathbb{T}_i\}$ must yield the victim class label for $\mathbf{x}_V^{p_i}$. There are two possible cases. One is when $\mathbb{T}_i \notin \mathcal{T}$ and the other is when $\mathbb{T}_i \in \mathcal{T}$. In case one, without losing generality, assume $\mathcal{T} = \{\mathbb{T}_{t_1}, \dots, \mathbb{T}_{t_k}\}$ with $0 < k < (n-1)$

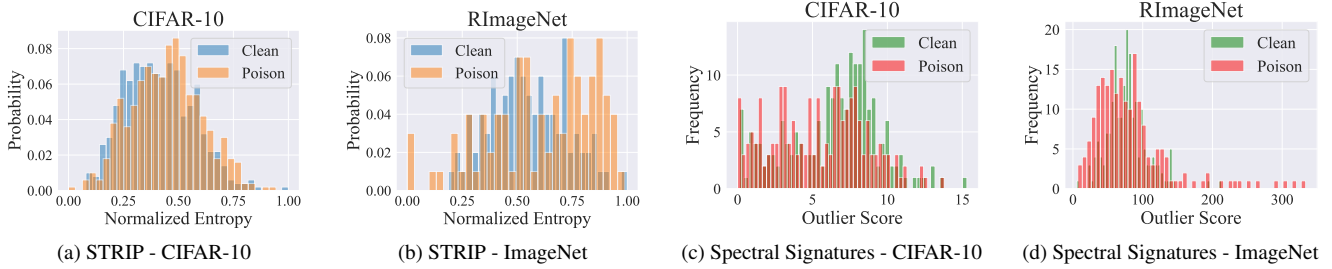


Figure 8. Evaluation against STRIP and Spectral Signatures on CIFAR-10 and ImageNet datasets.

and t_1, \dots, t_k not equal to i . As such, $\{\mathbb{T}_{t_1}\}, \dots, \{\mathbb{T}_{t_k}\}$ are the maximum subsets of \mathcal{T} regarding p_i . They have a consistent label y_V . As such, $\overline{\mathcal{M}}_{\bar{\theta}}(\mathcal{T} \oplus \mathbf{x}_V^{p_i}) = y_V$ based on the maximum subset Hypothesis (1).

In case two, without losing generality, assume $\mathcal{T} = \{\mathbb{T}_i, \mathbb{T}_{t_1}, \dots, \mathbb{T}_{t_k}\}$ with $0 < k < (n - 1)$ and t_1, \dots, t_k not equal to i . As such, $\{\mathbb{T}_i, \mathbb{T}_{t_1}\}, \dots, \{\mathbb{T}_i, \mathbb{T}_{t_k}\}$ are the maximum subsets of \mathcal{T} regarding p_i . They have a consistent label y_V . As such, $\overline{\mathcal{M}}_{\bar{\theta}}(\mathcal{T} \oplus \mathbf{x}_V^{p_i}) = y_V$. The hypothesis is hence proved. \square

E. Evaluation against Meta-classifiers

Table 7. Evaluation on ULP and MNTD.

# Partitions	2	3	4	5	6	7	Accuracy
ULP	0	1	0	0	0	0	16.7%
MNTD	1	0	1	1	0	0	50.0%

In this section, we evaluate LOTUS against backdoor detection methods based on meta-classifier, i.e., MNTD [80] and ULP [29]. Both methods aim to train a binary classifier from a large number of benign and poisoned models for backdoor scanning. They generate a set of input patterns and feeds them to the models whose output logits are then used to train the classifier. During training, the patterns and the binary classifier are optimized together in order to distinguish benign and poisoned models in the training set. During inference, these patterns are fed to the given model whose output logits are used by the binary classifier to decide whether the model is poisoned.

As MNTD and ULP require a large number of models for training, we adopt the TDC dataset², which consists of 125 benign models and 125 poisoned models trained on CIFAR-10 using WRN. We are able to train a MNTD and ULP classifier with over 90% training accuracy. To evaluate LOTUS against both meta-classifiers, we generate 6 poisoned models using the same dataset and structure, with 2-7 partitions. Table 7 presents the detection results by MNTD and ULP, where 0 denotes benign and 1 poisoned. Observe that the detection accuracy of ULP is only 16.7%, and MNTD 50.0%, showing they are unable to detect LOTUS.

F. Evaluation Against Testing-time Sample Detection

We conduct experiments to study the evasiveness of LOTUS against 2 testing-time sample detection techniques, STRIP [18] and Spectral Signatures [62] on a ResNet18 model trained on CIFAR-10 using K-means implicit partitioning and a VGG16 model trained on RImageNet using secondary labeling. Specifically, for each model, we randomly select 400 clean and 400 poisoned samples and assess their distributions according to different baselines.

STRIP [18] examines the entropy of the resulting predictions to identify the presence of a backdoor trigger by superimposing an input with a set of clean samples. The overlapping distributions of the normalized entropy for clean and poisoned data in Figure 8a and 8b indicate that LOTUS evades the detection of STRIP. The reason is that super-imposing breaks condition of correct partitions to trigger the backdoor. On the other hand, Spectral Signatures [62] identifies backdoor attacks by detecting outliers in feature covariance spectra through singular value decomposition. Figure 8c and 8d visualizes the distributions of outlier scores for clean and poisoned samples, where they highly overlap, meaning Spectral Signatures is unable to detect LOTUS’s poisoned samples. This is because LOTUS learns a complex mapping from partition secrets to trigger injection, making the internal values similar to that of complex benign features.

²<https://trojandetection.ai/>

G. Extension to Universal Attacks

We extend LOTUS to universal attack by partitioning samples based on their classes. Using ResNet18 as an example model, we divide CIFAR-10 samples into 5 partitions (2 classes for each partition) and apply Trigger Focusing for target label 0. We achieve 94.14% BA, 95.99% ASR and 5.94% ASR-other. Furthermore, the attacked model successfully evades the detection by NC, with an anomaly index of 1.614, which is below the established outlier threshold of 2.

H. Comparison with Additional Backdoor Attacks

We reproduce another two novel attack clean-label [64] and adaptive blend [48] on CIFAR-10 and ResNet-18 with over 94% BA and 99% ASR. NC can detect both of them and Fine-pruning can reduce their ASRs to <10%. However, NC and Fine-pruning cannot detect/mitigate LOTUS according to the results in Section 5.3 and Section 5.4, which indicates LOTUS outperforms these attacks regarding both evasiveness and resilience.

I. Evaluation against Additional Backdoor Mitigation Methods

We evaluate LOTUS on the two additional backdoor mitigation methods, i.e., I-BAU [15] and ARGD [14], using CIFAR-10 and ResNet-18. We create 4 victim partitions for LOTUS and assume the defender has access to 5% of the training data. Results are shown in Table 8, where we observe they are effective against the novel attack WaNet (ASR<10%), but fail to sufficiently defend LOTUS (ASR>30%). This is due to LOTUS’s unique backdoor mechanism that relies on benign partitions, posing a great challenge for these mitigation methods.

Table 8. Evaluation against additional defense

Defense	LOTUS		WaNet	
	BA	ASR	BA	ASR
No Defense	91.54%	93.80%	91.22%	98.57%
I-BAU	88.95%	38.60%	88.84%	9.21%
ARGD	88.18%	31.30%	89.92%	1.39%

J. Discussion about the ASR of LOTUS

LOTUS achieves around 93% ASR across various models and datasets (Table 1), slightly lower than state-of-the-art attacks, e.g., Ftrojan [13] and WaNet [46]. However, LOTUS shows greater resilience to defenses. For instance, novel defense ANP [72] only reduces LOTUS’s ASR to 35%, compared to under 3% for Ftrojan and WaNet, as shown in Table 9. We also explore a variant of LOTUS (LOTUS-rel.) by slightly reducing the weight on the dynamic loss (Equation 3). LOTUS-rel. increases ASR to over 98%, at a slight cost to resilience, reflecting a trade-off between ASR and resilience.

Table 9. Discussion about the ASR

Attack	No Defense		ANP	
	BA	ASR	BA	ASR
FtTrojan	91.53%	99.95%	88.64%	2.09%
WaNet	91.22%	98.57%	89.07%	0.54%
LOTUS	91.54%	93.80%	88.14%	34.90%
LOTUS-rel.	91.76%	98.20%	90.10%	27.97%

K. Adaptive Defense

In this section, we assess the performance of LOTUS under various adaptive defense scenarios. We operate under the assumption that defenders have knowledge about the victim class and the number of partitions implemented by LOTUS. With this information, they can independently create partitions and utilize existing defense strategies to reverse-engineer a trigger for each partition and conduct detection. To illustrate, we conduct experiments using the ResNet18 model on CIFAR-10 attacked by LOTUS, employing four partitions generated via the implicit partitioning using K-means. We leverage NC [67] as a typical baseline for detection against LOTUS on partitioned samples. A model with anomaly index exceeding 2, as produced by NC,

Table 10. Evaluation on adaptive defense.

Partition Method	Par. 0	Par. 1	Par. 2	Par. 3	MO
GT	2.587	1.985	2.366	2.841	100%
Inputs	1.178	0858	0.691	0.832	47%
Internals	1.358	0.699	1.387	0.905	67%

Table 11. Evaluation on other partitions.

Metrics	Half 0 + half 1	Half 2 + half 3	Equal 4	Random
NC index	1.316	0.823	1.041	1.019
MO	50%	50%	25%	27%

is considered backdoored. Table 10 displays the outcomes for different partitioning techniques. The first column denotes the partitioning methods, with “GT” implying that the defender possesses precise knowledge of the partitions, “Inputs” suggesting that the defender employs K-means to generate partitions from input samples, and “Internals” meaning the defender utilizes K-means to partition based on internal feature representations. Subsequent columns represent NC anomaly indexes generated on various partitions. The last column, “MO” quantifies the maximum overlap between generated partitions and one of the ground-truth partitions. We observe that if defenders possess knowledge of the ground-truth partitions, they have a higher likelihood of detecting LOTUS by using samples from a specific partition. However, it is often impractical for defenders to have such knowledge. Scenarios where defenders generate partitions from input or feature data are more realistic. However, even when defenders employ the same partitioning algorithm on input samples and feature representations, they face difficulties in detecting LOTUS. This is because LOTUS leverages a surrogate model to learn partitioning principles, rather than directly using K-means results. Consequently, their partitioning outcomes differ, with an MO of only 67%. Table 11 presents additional results, testing detection scenarios where samples consist of an equal mix from two partitions (Half 0 + half 1), an equal mix from all four partitions (Equal 4), or random selections from partitions. In all instances, defenders find it challenging to detect LOTUS. In conclusion, even when defenders possess prior knowledge of LOTUS, detecting the backdoor remains challenging due to the complexity of its sub-partitioning approach.

L. Ablation Study

In this section, we conduct a series of ablation studies of LOTUS on different settings and hyper-parameters.

Table 12. Results w/ and w/o surrogate models.

Method	BA	ASR	ASR-other
K-means	94.36%	84.40%	19.01% ± 39.24%
K-means + surrogate	94.71%	94.30%	4.39% ± 17.08%
GMM	94.78%	86.38%	20.51% ± 40.38%
GMM + surrogate	94.59%	90.70%	4.80% ± 21.38%

L.1. Necessity of Using Surrogate Models

We verify the necessity of training a surrogate model for implicit sub-partitioning to attain high attack effectiveness with LOTUS. To validate this, we conducted experiments utilizing the ResNet18 model on CIFAR-10 and compared the attack performance achieved through traditional partitioning methods, specifically K-means and GMM, with the performance achieved when training a surrogate model for partitioning. The outcomes are presented in Table 12.

Notably, when we omit the surrogate model, the ASRs experience a noteworthy reduction, ranging from 4% to 10%. Additionally, ASRs-other exhibit an increase. This decline in performance is due to the difficulty of the attacked model to effectively learn the traditional partitioning schemes. This also highlights the necessity of training a surrogate model for sub-partitioning to achieve good attack performance.

L.2. Effect of Different Number of Partitions

We evaluate the attack’s effectiveness by generating different numbers of partitions. The experiment is conducted on ResNet18 trained on CIFAR-10 using implicit sub-partitioning. The results are shown in Figure 9, with the x-axis representing the number of partitions and the y-axis indicating the percentage values for different metrics. These metrics include BA (Backdoor

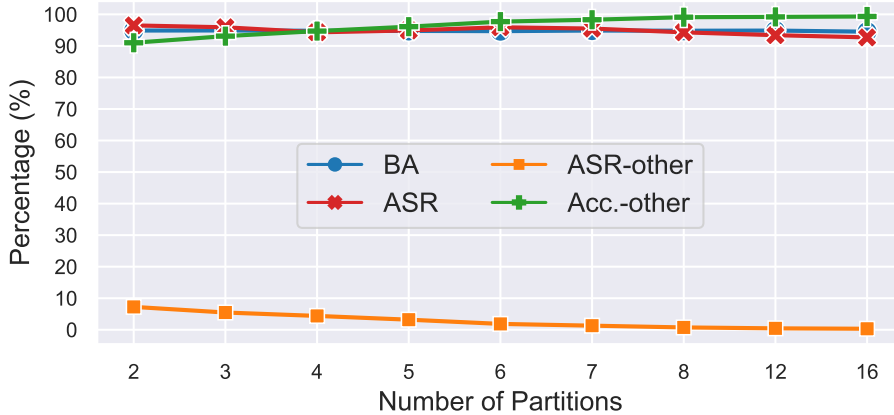


Figure 9. Attack effectiveness of different number of partitions

Accuracy), ASR (Attack Success Rate), ASR-other (Attack Success Rate of images assigned incorrect triggers), and Acc.-other (Accuracy for images with incorrect triggers).

It is noteworthy that BAs and ASRs consistently remain at high levels, showcasing the attack’s effectiveness across various partition numbers, even when the number of partitions is as high as 12 or 16. Additionally, ASR-other values are low, while Acc.-others values are high, indicating that images marked with incorrect triggers tend to be predicted as belonging to their source labels. This observation further indicates that LOTUS achieves good performances across various partition counts.

Table 13. Results on different number of samples per partition.

# Samples per Partition	BA	ASR	ASR-other
1000 (default)	94.74%	93.90%	5.65%
500	93.94%	90.70%	7.09%
250	94.45%	91.20%	5.77%
100	92.00%	81.10%	9.46%
50	89.46%	79.40%	8.64%

L.3. Effect of Different Number of Samples per Partition

We explore the influence of different sample counts per partition, a crucial factor when employing sub-partitioning within the victim class. First, unevenly distributed samples resulting from partitioning could introduce fairness issues in learning. To mitigate this, we analyze the post-partitioning sample counts and strive to maintain a roughly balanced distribution, although sample imbalance rarely occurs (as discussed in Section 4.1).

Another potential challenge arises when the number of samples per partition is limited, potentially affecting trigger focusing due to the requisite knowledge of sub-partitioning secrets. To examine this effect, we conducted experiments using ResNet18 models on the CIFAR-10 dataset, generating 4 partitions within victim class 0. The results are displayed in Table 13, with the first column representing the number of samples per partition, followed by benign accuracy (BA), attack success rate (ASR), and attack success rate for non-targeted triggers (ASR-other). We compare LOTUS’s performance with the default setting of 1000 samples per partition and other configurations. It is notable that as the number of samples per partition decreases, both BA and ASR exhibit declines, while ASR-other experiences an increase. These results indicate that LOTUS’s performance degrades with fewer samples per partition. However, it’s worth highlighting that even with just 250 samples, an ASR of over 91% can be achieved. This suggests that LOTUS generally requires around 1000 samples per victim class for good performance, which is often practical across various datasets.

L.4. Effect of Different Victim-Target Class pairs

In the previous experiments, we use the first class as the victim and the last class as the target as the default setting. Here, we randomly select a few victim-target class pairs to study how they affect the performance of LOTUS. We conduct an experiment on ResNet18 on CIFAR-10 and use implicit sub-partitioning to generate 4 partitions. Table 14 shows the results. Observe that LOTUS consistently has a high ASR with different victim-target class pairs, and the ASR-other values are relatively low, delineating the generalizability of LOTUS to different class pairs.

Table 14. Results on different victim-target class pairs.

Victim	Target	BA	ASR	ASR-other
0	9	95.01%	91.40%	4.65% ± 16.06%
4	5	94.94%	93.10%	3.64% ± 18.74%
1	6	95.13%	95.70%	5.44% ± 22.67%
7	4	95.03%	93.40%	5.89% ± 23.55%
3	2	95.21%	89.60%	6.38% ± 24.44%

Table 15. Results on different trigger patterns.

Trigger Pattern	BA	ASR	ASR-other
Color Patch	95.01%	91.40%	4.65% ± 16.06%
Logo	94.89%	91.40%	4.63% ± 16.00%
Instagram Filter	94.40%	89.10%	6.90% ± 21.24%

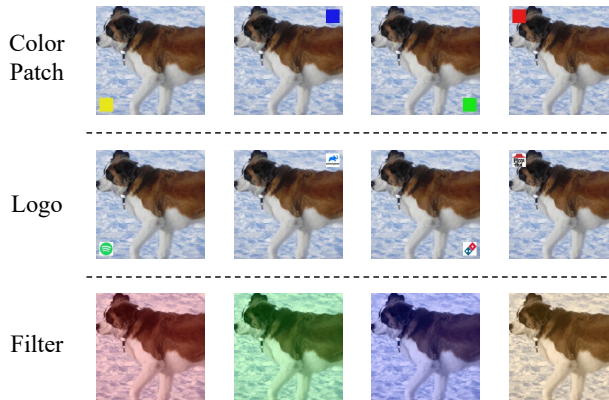


Figure 10. Different trigger patterns. The first row shows the color patch triggers, the second row logo triggers and the third row Instagram filter triggers.

L.5. Effect of Different Triggers

We use solid polygon patches as triggers in our previous experiments. We study two other types of triggers, logos and Instagram filters. Figure 10 shows different trigger patterns. The first row shows the color patch triggers, the second row the logo triggers (downloaded from the Internet), and the third row the Instagram filter triggers. We use a ResNet18 model on CIFAR-10 with 4 partitions for the study. Table 15 presents the results. All three studied cases have high BAs, ASRs, and low ASRs-other. Due to the overlapping of triggers during trigger focusing, there is a slight degradation of the attack effectiveness on Instagram filter, with 2% ASR degradation and 2% ASR-other increase. The Instagram filter cases perturb the entire image and hence slightly degrade the performance of trigger focusing. Overall, LOTUS is effective with different types of triggers.

Table 16. Results on different patch sizes.

Patch Size	BA	ASR	ASR-other
3 × 3	94.80%	93.90%	4.32%
6 × 6	94.89%	94.30%	4.39%
10 × 10	94.40%	94.40%	5.09%

L.6. Effect of Different Patch Trigger Sizes

We study the effect of different trigger sizes using solid patches as the trigger. We conduct experiments on ResNet18 model on CIFAR-10 with 4 secret partitions. We evaluate patch sizes of 3 × 3, 6 × 6 and 10 × 10. Results are shown in Table 16, where the first column denotes the trigger sizes with the subsequent columns illustrating LOTUS’s performance, i.e., BA, ASR and ASR-other. Observe that LOTUS is generally effective using multiple trigger sizes, with high benign accuracy, ASR and low ASR-other.

Table 17. Results on different pre-trained encoders.

Encoder	BA	ASR	ASR-other
VGG	94.71%	94.30%	4.39% \pm 17.08%
AlexNet	95.10%	92.70%	4.59% \pm 20.92%
SqueezeNet	94.75%	91.60%	4.26% \pm 20.21%

L.7. Effect of Different Pre-trained Encoders

In the previous experiments, we leverage the pre-trained encoders of VGG [84] to extract features of victim samples. We study other two encoders of different structures. We conduct experiments on a ResNet18 model on CIFAR-10 with 4 implicit partitions. Table 17 shows the results of using different pre-trained encoders. Observe that LOTUS achieves a consistent good performance through out all encoders.

M. Evaluation Against GradCAM

The GradCAM [53] method is commonly used to visualize the important regions of inputs through gradient propagation. In this study, we evaluate LOTUS using GradCAM and compare the results with those of BadNets [19] and Dynamic [51] backdoors. Figure 11 displays the results, which are organized into four groups of images representing the GradCAM visualizations for the clean model, the BadNets attacked model, the Dynamic attacked model, and the LOTUS attacked model. In each group of images, the first row shows the poisoned images (clean images for the clean model), while the second row shows the GradCAM visualizations. The reddish regions represent important areas, while the bluish regions represent less important parts.

Our observations revealed that for both BadNets and Dynamic backdoors, the important regions are located at the trigger positions, indicating that their triggers have notable features regarding the gradients. However, for LOTUS’s poisoned images, the important regions are more similar to those of the clean models. This further validates the evasiveness of LOTUS and explains why it is difficult to be inverted.

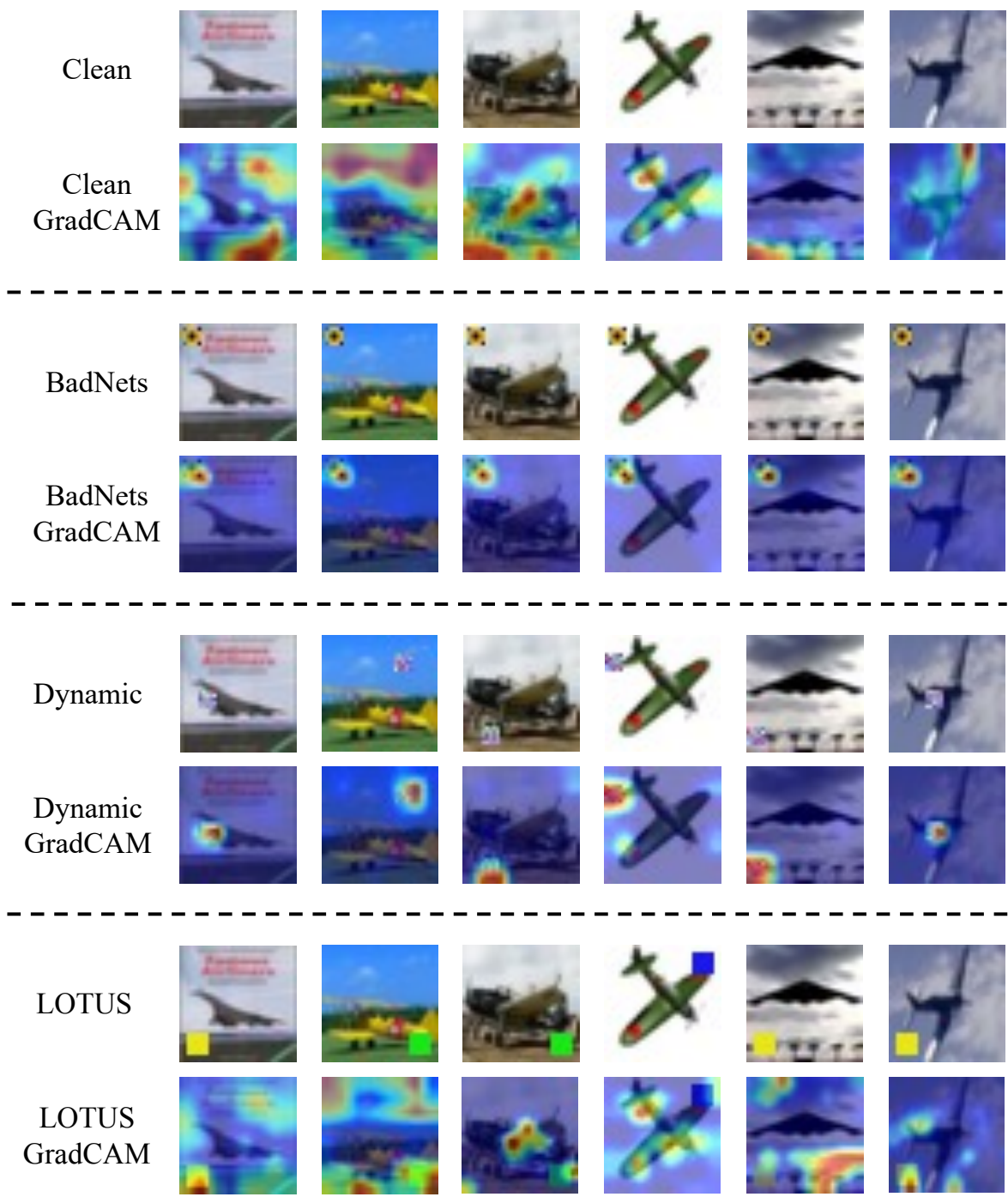


Figure 11. Important region visualizations via GradCAM.